1-1-2005

Fatigue response of aircraft wing root joints under limit cycle oscillations

Behzad Yousefirad
Ryerson University

Ryerson University

Faculty of Engineering and Applied Science

School of Graduate Studies

Mechanical Engineering Program

Fatigue Response of Aircraft Wing Root Joints Under Limit Cycle Oscillations

by
BEHZAD YOUSEFIRAD

A project
presented to **Ryerson University**

in partial fulfillment of the

requirement for the degree of

Master of Engineering
in the program of

Mechanical Engineering

Toronto, Ontario, Canada, 2005

Author's Declaration
I hereby declare that I am the sole author of this project.

I authorize Ryerson University to lend this project to other institutions or individuals for the purpose of scholarly research.

* Signature

I further authorize Ryerson University to reproduce this project by photocopying or by other means, in total or in part, at the request of other institutions or individuals for the purpose of scholarly research.

* Signature

Abstract

When wing root attachments are subject to cyclic loading during a flight, slipbands are produced by fatigue. The density of these slipbands increases with the advancing of the fatigue process and initial cracks appear within the persistent slipbands. This project investigates the fatigue response of a titanium alloy wing root joint under different loading spectra during limit-cycle oscillations by the strain-life approach.

Although wing root attachments are designed such that the nominal loads remain elastic, stress concentrations often cause plastic strains to develop in the vicinity of notches. Subsequently, wing loads caused by limit-cycle oscillations lead to fatigue damage accumulation.

This project's results lead to the conclusion that cyclic loading during limit-cycle oscillations can cause fatigue damage in wing root joints. Tensile mean stress is detrimental to the fatigue life of wing root joints, while compressive mean stress is beneficial.

Acknowledgements

The author would like to express his great gratitude to his supervisor, **Dr. Hekmat Alighanbari**, for his immense guidance and continuous support throughout the course of his graduate studies. He was fortunate to receive affirmative comments, stimulating ideas and understanding from him that made this project a success.

Many thanks are due to Dr. Cheung Poon for his constructive comments and stimulating discussions.

Sincere thanks go to the author's parents and wife for their kindness and continuous supportive encouragements.

Table of Contents

Table of Contents (Continued)

List of Tables

List of Illustrations

Nomenclature

a_1	Effective crack half length
$2a$	Total crack length
b	Fatigue strength exponent = Slope of the elastic strain curve
c	Fatigue ductility exponent = Slope of plastic strain curve
E	Modulus of elasticity
FAR	Federal Aviation Regulations
HCF	High Cycle Fatigue
K	Stress intensity factor
LCF	Low Cycle Fatigue
LCO	Limit Cycle Oscillations
n_j	The number of cycles applied at a load corresponding to a lifetime of N_j
N_f	Fatigue life (cycles)
$N_{f.j.}$	Fatigue life corresponding to stress cycle j
$2N_f$	Fatigue life (reversals)
N_j	Fatigue life
S_e	Endurance limit = Fatigue strength = Allowable stress
$\varepsilon_f^{'}$	Fatigue ductility coefficient
$\Delta\varepsilon_e$	Elastic strain range
$\Delta\varepsilon_p$	Plastic strain range
σ_a	Alternating (amplitude) stress
$\sigma_f^{'}$	Fatigue strength coefficient
σ_m	Mean stress
$\Delta\sigma$	Total stress range

1. Introduction

Fatigue is a process in which damage accumulates in a component due to repetitive application of loads that may be well below the yield point. The process is dangerous because a single application of the load would not produce any ill effects, and a conventional stress analysis may lead to an assumption of safety that does not exist.

Fatigue occurs when an element of a structure is subject to cyclic stresses over a long period of time. Some examples of where fatigue may occur are: aircraft wings and fuselage, helicopter rotor blades, turbine blades, etc.

The wing is one of the most critical parts of an aircraft. This critical part has attracted a great deal of attention in the engineering literature but only a minor part of this attention has been paid to fatigue of wing root joints, although these joints are one of the most critical areas in the aircraft's structure, in particular for fatigue considerations.

Limit cycle oscillations (LCOs) are oscillations with limited amplitudes that may occur on a wing. Uniform growth of wing oscillations to constant amplitude is the sign of limit cycle oscillations. Since the fatigue-LCO relationship is still in the early stages of research, it needs further investigations and analyses. Little is known or at least written about this cause-and-effect relationship in a flight vehicle. Interestingly enough, to the author's knowledge virtually nothing quantitative has been published in this regard.

The focus of this project is to investigate the fatigue response of a wing root joint under different loading spectra during limit-cycle oscillations by the strain-life ($\varepsilon - N$) approach. Although wing root attachments are designed such that the nominal loads remain elastic, stress concentrations often cause plastic strains to develop in the vicinity of notches, and consequently, wing loads caused by LCO lead to fatigue damage accumulation in wing root attachments.

The goals of this project are:

- To investigate if cyclic loading during limit-cycle oscillations can cause fatigue damage in wing root joints.

- To find out the effect of tensile and compressive mean stresses on the fatigue life of wing root joints.

This project is organized as follows. It will first review the loads on a wing briefly. It will then provide brief insights for wing structure of fixed-wing aircraft. A brief description of wing root joints and preferred arrangements (lug/pin attachment) is also given. Relevant fatigue theories as well as limit cycle oscillation phenomenon are discussed.

Chapter 12 introduces five loading spectra, which are concerned with a lug/pin attachment of a fighter jet wing during LCO. In loading # 1 the wing root joint is subjected to a cyclic loading spectrum due to LCO. Calculations presented in Chapter 12 indicate that loading # 1 is in the plastic region, and the specified wing root joint has a short fatigue life (LCF). The same lug/pin attachment is then allowed to experience various loading spectra to estimate fatigue life of the joint. The loading spectra are demonstrated in loading # 2 to loading # 5. Based on the calculations the specified wing root joint experiences plastic deformation. It is shown that depending on the magnitude of load spectrum, this plastic deformation causes fatigue damage. Loadings # 4 and 5 show elastic behaviour which imply infinite fatigue life for the lug/pin attachment. In Chapter 13 the strain-life (ε - N) curve is calculated and plotted for the lug/pin arrangement of a fighter jet wing. In Chapter 14 the mean stress effect on fatigue life of the joint is illustrated in detail through applying loading spectra during LCO with constant stress amplitude.

2. Wing Loads and Wing Structure

2.1. Wing Loads

Aircraft wings are subject to several distributed and concentrated loadings including aerodynamic, gust, landing, weight and engine loadings. These loads cause internal loads in the wing structure. A wing structure for any aircraft has to be designed to cope with these loads, while at the same time being sufficiently light in weight and generating enough lift so the aircraft can take off. That means required properties of wing structure must include: flexural stiffness (along the wing), torsional stiffness and light in weight.
Bending, torsional, shear, axial, compressive and tensile loads are considered as internal loads. A wing structure experiences a combination of these loads.

2.2. Wing Structure

2.2.1. Wing Structure Synthesis

In the 1930's, the Lancaster Bomber used the section of wing as shown in Fig. 2.2.1.1. It had 2 spars which ran down the length of the wing and booms where the spars met the wing cover. All the strength of the wing came from the spars and the booms.

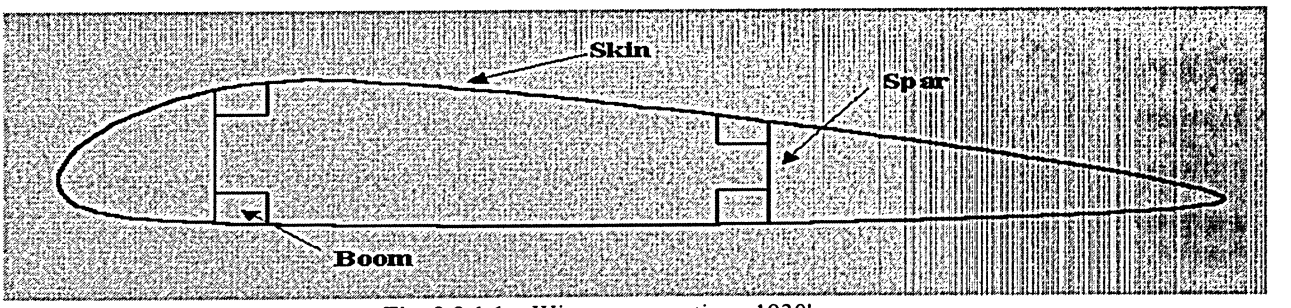

Fig. 2.2.1.1 – Wing cross-section , 1930's

In the 1950's (Fig. 2.2.1.2) wing skin became a load bearing member of the structure. It took some of the stresses in the wing and therefore the structure inside the wing did not have to take so much of the stress and could be lighter.

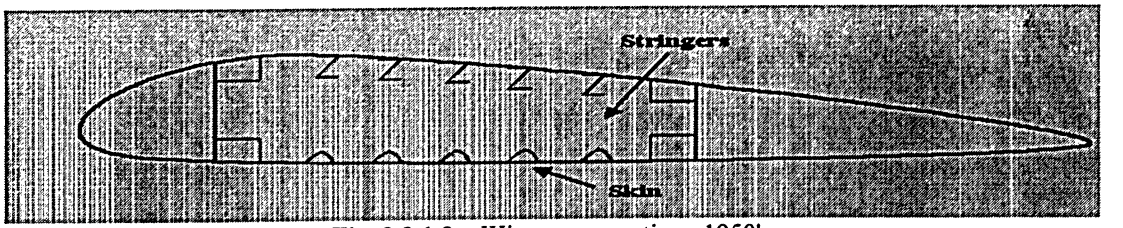

Fig. 2.2.1.2 – Wing cross-section , 1950's

By the 1980's, wings were designed so that every part of the wing had a structural purpose, thereby reducing the weight of the wing. The design is called a "torsion box" design. The torsion box (Fig.2.2.1.3) runs along the length of the wing, providing all the torsional stiffness and longitudinal stiffness required in the wing [20]. The torsion box is made up from the skin of the wing, spars at both ends, and stringers.

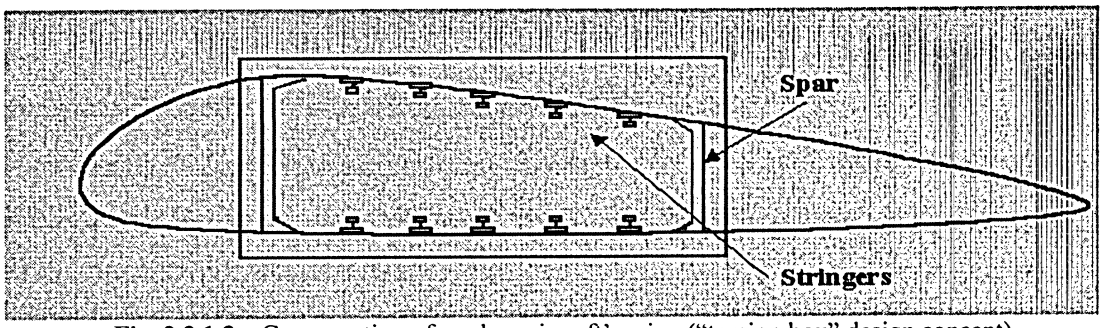

Fig. 2.2.1.3 – Cross-section of modern aircraft's wing ("torsion box" design concept)

3. Wing-Fuselage Intersection

Fig. 3.1 illustrates wing-fuselage intersections. This intersection is called a "carry-through section". The mid-wing type is mostly used for military fighter jets. Fig. 3.1 (c) is the case for many fighter jets. In this kind of mid-wing design, the wing box structure does not allow one to carry through the fuselage structure, therefore heavy forging structures are designed to carry through the wing loads.

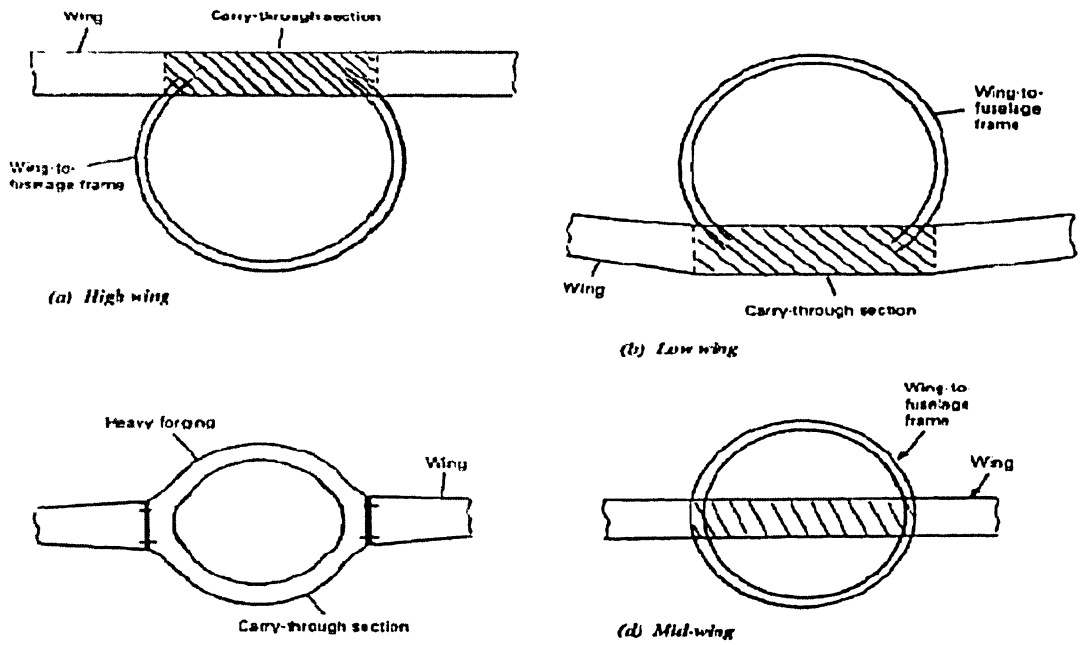

Fig. 3.1. Wing-fuselage intersection (carry-through section) [5, p. 406]

3.1. Wing-Fuselage Connection

The wing-Fuselage connection presents some very interesting design problems. The four-pin design concept for B707 transport during 1950s is simple and straightforward (see Fig. 3.1.1).

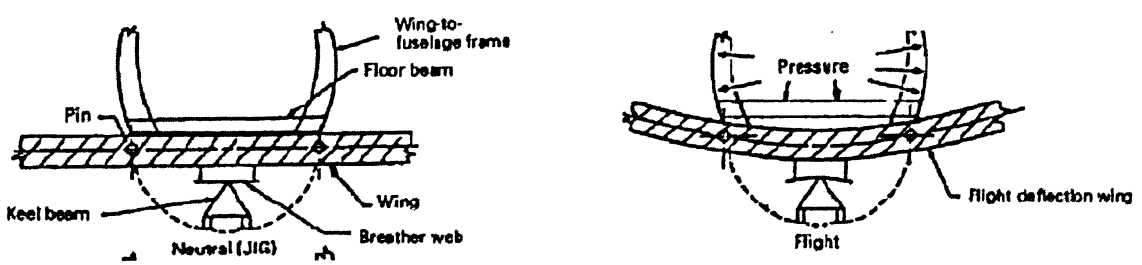

Fig. 3.1.1. B707 wing-fuselage connection [5, p. 408]

The lift and moment loads can be carried between the wing and fuselage by shear on 4 pins, but there is another load vector to be considered: drag and thrust (fore and aft load) which is taken by a breather web [5, p.408]. This design allows the wing spar and fuselage bulkheads to deflect independently of each other so that no spar moment is directly transferred to the bulkheads.

A typical design of a modern transport wing-fuselage connection is to bolt the main frame to both front and rear spars of the wing box. This type of connection has been widely used by aircraft designers for many years, and the detailed design should be capable of sustaining the fatigue loads due to the deflection imposed by the wing bending. Fig.3.1.2 shows that both spar moment and shear connections are spliced into the fuselage forward and aft bulkheads. The bulkhead and wing spar are rigidly connected together as one integral unit which has been chosen primarily to save structural weight.

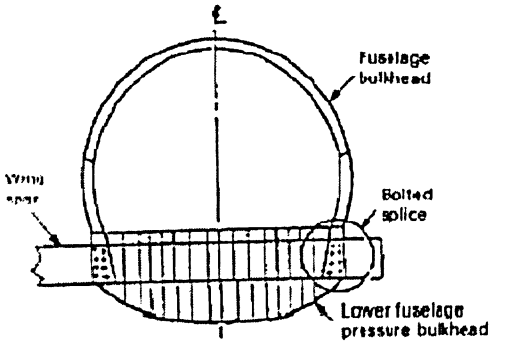

Fig. 3.1.2. Integral unit of fuselage bulkhead & wing spar [5, p. 410]

This type of construction (Fig. 3.1.2) utilizes the elastic characteristics of related parts and requires sophisticated finite element analysis technology [5, p.409]. A material that is perfectly elastic within the range of stress applied to it, will not suffer fatigue; when fatigue occurs, it must be associated with inelastic deformation during each stress cycle [2, p.63].

Fig.3.1.3 illustrates the fuselage frame and bulkheads connected to stub floor beams over the wing center section box and wing spars. It is obvious that the deep floor beam imposes a much greater load on the frame, a fact proved by frame failure experienced in aircraft with relatively low service time. The point is not to overlook the loads induced by structural deflections or instability of supporting or attaching structures. A fatigue-crack sensitive area is

circled in Fig. 3.1.3. Wing deflection during up-bending and down-bending which could cause premature fatigue cracks is identified by dashed lines.

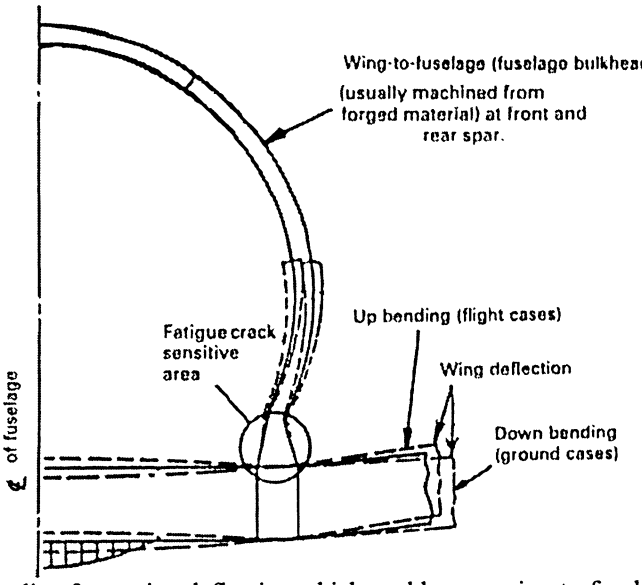

Fig. 3.1.3. Induced frame bending from wing deflection which could cause wing-to-fuselage main frame premature fatigue cracks [5, p. 410]

4. Wing Root Joints and Attachments

Wing joint design is one of the most critical areas in aircraft structures, in particular for fatigue consideration of long life structure.

There are basically two types of wing joint design, (i) fixed joint and (ii) rotary joint. Rotary joints are utilized for variable swept wing aircraft. They are not discussed in this report since they are beyond the scope of this project. Advantages and disadvantages of different fixed joints are summarized in Table 4.1.

Joint	Advantages	Disadvantages
Spliced plates	Widely used due to its light weight and more reliable and inherent fail-safe feature	Slightly higher cost, manufactural fitness required
Tension bolts	Less manufactural fitness required, easy to assemble or remove. More economic for military fighter with thin airfoil.	Heavy weight penalty
Lug/pin	Less manufactural fitness required, easy to assemble or remove. More economic for military fighter with thin airfoil.	Heavy weight penalty
Combination of spliced plates & tension bolts	Reliable and inherent fail-safe feature, and less manufactural fitness required.	Heavy weight penalty

Table 4.1. Wing root fixed joints

The best fatigue design, of course, is one with no joints or splices. This is accomplished on the modern transports which have no joints across the load path except at the side of the fuselage [5, p.282]. Wing sweep plus dihedral and manufacturing joint requirements make the joint at the side of fuselage necessary. It is important to keep the joint short. A long joint tends to pull load in, from adjoining areas.

Fig. 4.1 illustrates a lug/pin attachment for a fighter jet. This design configuration is a highly loaded wing root joint. The lug/pin attachment as shown in Fig. 4.1 is widely adopted in aircraft wing designs because of good load transfer without excessive stress concentration.

This characteristic contributes in ensuring fatigue life. The high structural efficiency of the lug/pin attachment is another reason to attract designers attention during wing root design process.

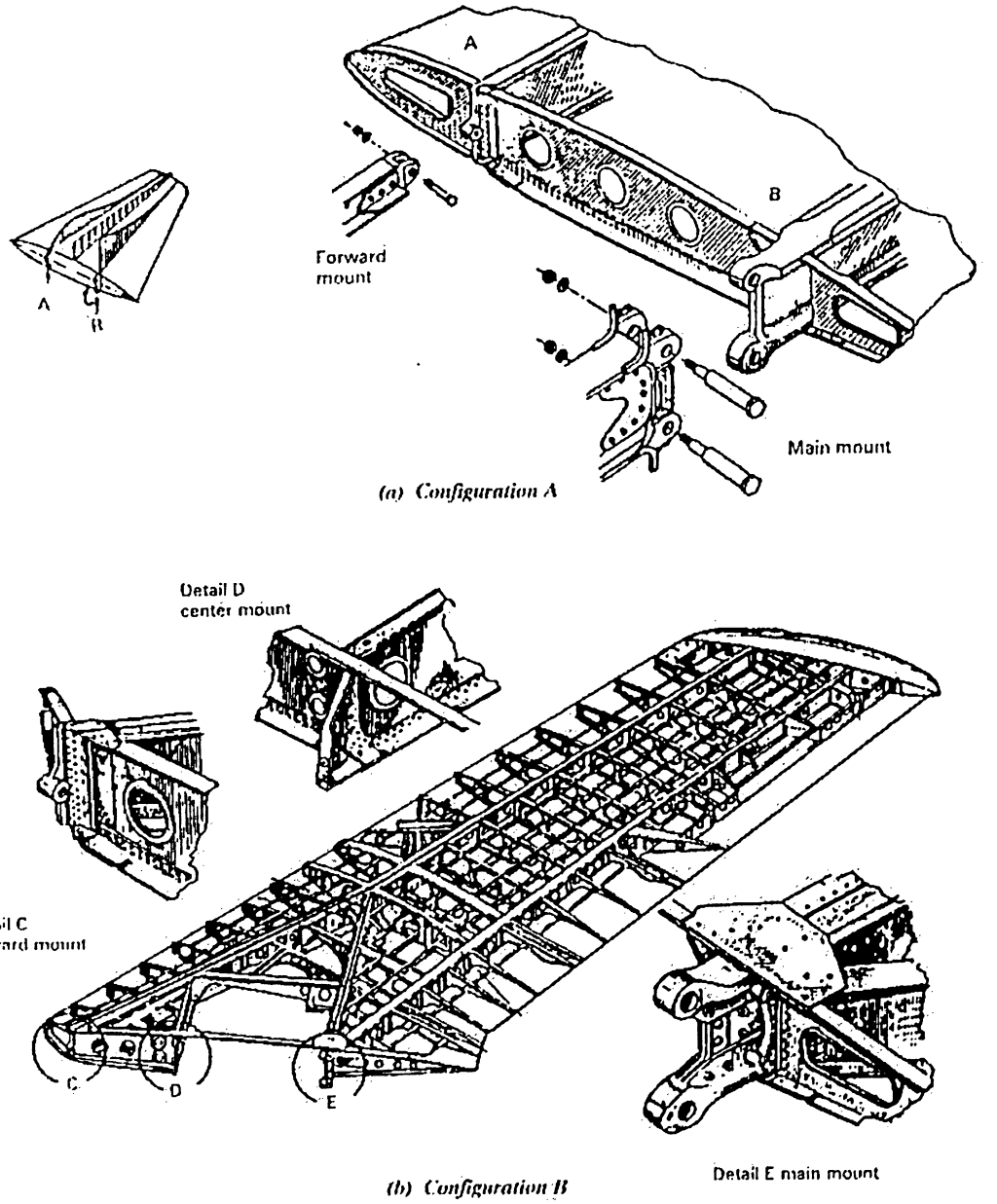

Fig. 4.1. Lug/pin arrangement. Detail E shows one of the lugs [5, p. 288]

Most of the lightly loaded wings for general aviation aircraft adapt a single main front spar and an auxiliary rear spar construction. Therefore, the wing root joint usually is a triple point

lug joint as illustrated in Fig. 4.2. The upper and lower lugs at the front spar pickup wing bending loads, vertical shear loads and wing torque; the single lug at the auxiliary rear spar takes wing vertical shear loads and torque only.

If it is a highly swept fighter wing, the rear spar should be the main spar and the front spar is the auxiliary spar [5, p.286]. To ensure fatigue life and structural integrity, these lugs generally are machined from forging materials which is not only to reduce weight but also to minimize the local stress concentration. The double shear design as shown in Fig. 4.2(d) has to apply to all lug construction to obtain the most efficient joint.

Fig. 4.2(d) illustrates a fail-safe design feature of "bolt within a hollow tube" which is used in lug/pin arrangements. In case the hollow tube fails the bolt will take the load.

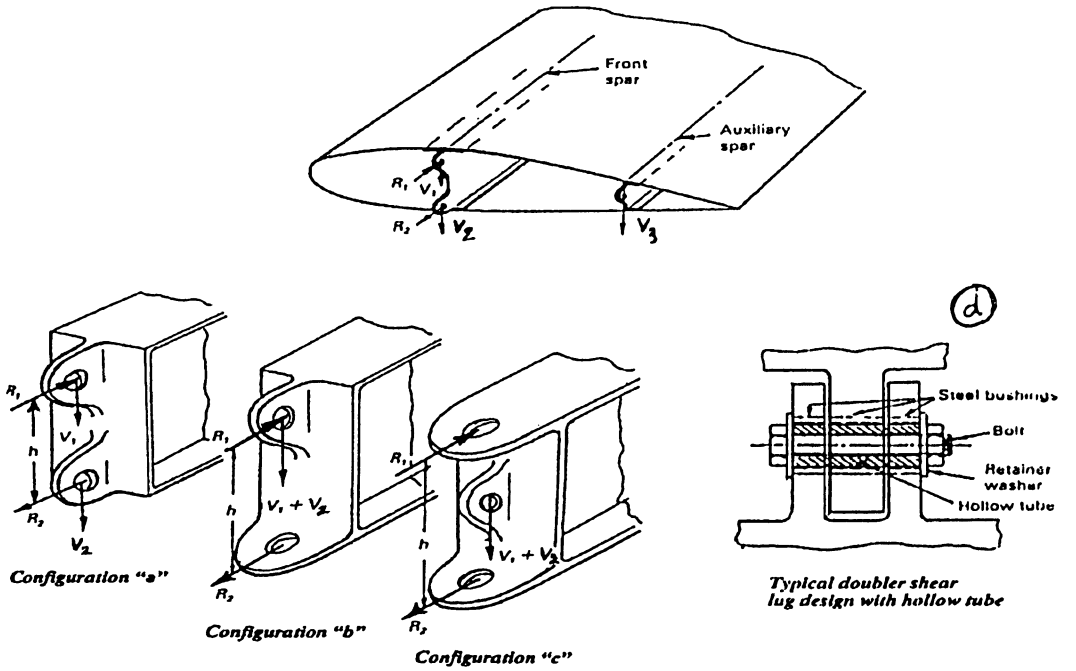

Fig. 4.2. Wing lug/pin design configuration and comparison [5, p. 287]

5. Stress Analysis Approaches for Fatigue Analysis of Wing Root Joints

Three major categories might be envisioned for stress analysis applications that are used for fatigue analysis of wing root joints: (i) Experimental methods, (ii) Finite element analysis (FEA), (iii) Analytical methods.

An analytical approach is taken in this project. Analytical methods attempt to resolve a problem into elements or constituent parts. Many classic engineering courses such as fatigue analysis, engineering mechanics and strength of materials are classified in this category.

Analytical methods are also widely used to verify or compare the results of other methods of analysis. For instance, elementary beam theory can be used to verify the accuracy of results of a finite element analysis for a cantilever beam.

6. Limit Cycle Oscillations (LCO)

The title of this project is "*Fatigue Response of Aircraft Wing Root Joints under Limit Cycle Oscillations*". A brief description and definition of this aerodynamic phenomenon is given in this chapter.

Flutter is a dangerous phenomenon encountered in flexible structures subjected to aerodynamic forces. This includes aircraft, buildings, telegraph wires, and bridges. In the case of an aircraft, flutter is of particular concern due to the inherent flexibility of the structure and extreme aerodynamic loads experienced.

Aerodynamic and structural nonlinearities may provoke an aeroelastic behavior that is referred to as LCO. Compared to "classical" flutter, where the amplitudes of the structural vibrations grow exponentially at flight speeds above the critical flutter speed until the structure fails, LCOs are oscillations with limited amplitudes.

LCO is characterized by rather constant amplitude periodic structural response at selective frequencies, which are usually recognizable as being those of the aeroelastically loaded structure. Uniform growth of wing oscillations to constant amplitude is the signature of LCO.

Bunton and Denegri [39] discuss LCO characteristics of fighter aircraft, and Denegri [40] provides test cases from flight tests of the F-16 aircraft for three classes of response: Classical Flutter, Typical LCO, and Nontypical LCO.

LCO occurrences are common on fighter aircraft; Norton [41] describes incidents on F-5, F-16, F-111, F-15 STOL, and F/A-18 aircraft. LCOs induced by structural nonlinearities have been widely reported in the literature.

Incidents of LCO are not limited to fighter aircraft. LCOs are reported by Jacobson, et al. [42] and Dreim, et al. [43] involving wing-bending interaction with rigid body pitching and plunging on the B-2 bomber, and Edwards [44] reports LCO on a generic business jet wind-tunnel flutter model.

LCO has been observed in flight operations of modern aircraft, wind tunnel experiments and mathematical models.

Fig.6.1(a) presents a wing's pitch amplitude response versus air speed during LCO [34]. Fig. 6.1(b) illustrates maximum stress response versus pitch amplitude. This means as aircraft speed increases during LCO, pitch angle tends to increase exponentially (Fig. 6.1.a). Likewise, as pitch angle increases, stress level tends to boost exponentially which impose higher stress intensity on wing root joints (Fig. 6.1.b). Hence, as aircraft speed changes the amplitude and frequency of LCO changes accordingly.

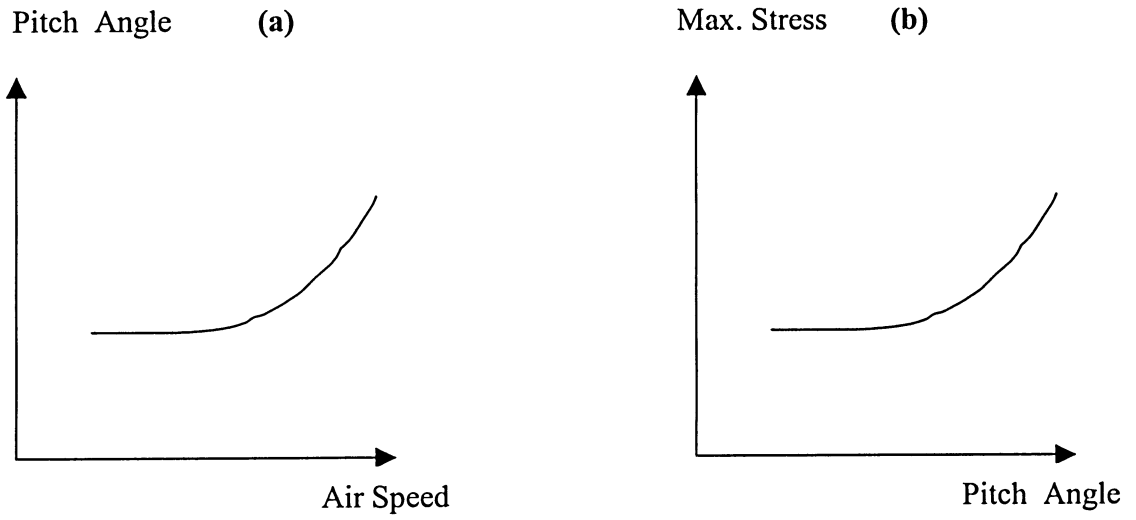

Fig. 6.1. (a) Pitch amplitude response versus air speed [34]; (b) Max. stress response versus pitch amplitude

7. Crack Initiation and Propagation

Although adequate precautions are taken to ensure that an aircraft structure possesses sufficient strength to withstand the most severe expected gust or manoeuvre loads, there still remains the problem of fatigue. The aircraft industry has led the effort to understand and predict fatigue crack growth. Practically, all components of the aircraft structure are subject to fluctuating loads which occur a great many times during the life of the aircraft. It has been known for many years that materials fail under fluctuating loads at much lower values of stress than their normal static failure stress. Fatigue is the primary reason that wing root joints fail catastrophically in service. The reason behind many maintenance practices and recommendations will be understood better with the knowledge of fatigue.

Fatigue happens when a repeated application of a load, eventually damages the atomic bonds between the material grains and causes cracks to form and grow. Further repetition of the load causes the crack to propagate further, thus weakening wing root joint and eventually causing failure. Failure of a material due to fatigue might be reviewed on a microscopic level in three steps:

(i) Crack Initiation: The initial crack occurs in this stage. The crack may be caused by surface scratches caused by handling, or tooling of the material; threads; slip bands or dislocations intersecting the surface as a result of previous cyclic loading or work hardening.

(ii) Crack Propagation: The crack continues to grow during this stage as a result of continuously applied stresses.

(iii) Failure: Failure occurs when the cracked material can not withstand the applied stress any more. This stage happens very rapidly.

Fig. 7.1 is a diagram showing the location of the three stages in a fatigue fracture under axial stress.

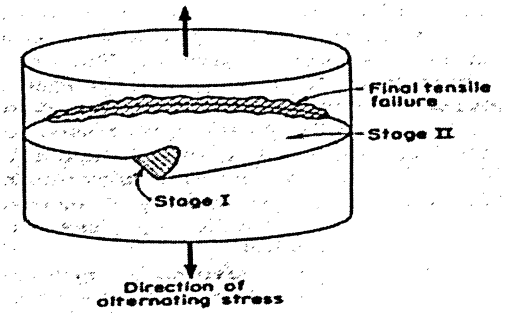

Fig. 7.1. Location of the three stages in a fatigue fracture under axial stress [48, p. 761]

8. Fatigue Crack Growth Rates (Propagation Rate)

If a wing root joint contains a crack, and if a cyclic or repeated load is applied, then the crack is likely to grow slowly with increasing number of load cycles. This process is known as fatigue crack growth. Once a fatigue crack is formed, the propagation rate of a crack is strongly influenced by load history and environmental factors. Thus, the accurate prediction of fatigue life is a complex problem. In a fatigue crack growth experiment, the progress of a crack growing under a cyclic load is measured, and the results are plotted as a fatigue crack growth rate curve, *da/dN* versus *K* (that is, change in crack length divided by change in number of cycles to failure versus change in fracture toughness). A typical fatigue crack growth curve is shown in Fig. 8.1.

It is vital that engineers be able to predict the rate of crack growth during load cycling so that the wing root joint can be replaced or repaired before the crack reaches a critical length. A great deal of experimental evidence supports the view that the crack growth rate can be correlated with the cyclic variation in the stress intensity factor.

$$\frac{da}{dN} = C.\Delta K^n \qquad \text{Eq. 8.1}$$

$$\Delta K = K_{max} - K_{min} = Y.\Delta\sigma\sqrt{\pi.a} \qquad \text{Eq. 8.2}$$

where *da/dN* is the fatigue crack growth rate per cycle, $\Delta K = K_{max} - K_{min}$ is the stress intensity factor range during the cycle, and *C* and *n* are parameters that depend the material, environment, frequency, temperature and stress ratio. This is also known as the "Paris law" and leads to plots similar to that shown in Fig. 8.1.

Re-arrangement and integration of Eq. 8.1 gives us the relation of the number of cycles to failure, N_f, to the size of the initial flaw length, a_0, and the critical crack length, a_C, and Eq. 8.2:

$$N_f = \int_0^N dN = \int_{a_0}^{a_C} \frac{da}{A.(Y.\Delta\sigma.\sqrt{\pi.a})^n} = \frac{1}{A.\pi^{n/2}.(\Delta\sigma)^n} \int_{a_0}^{a_C} \frac{da}{Y^n.a^{n/2}} \qquad \text{Eq. 8.3}$$

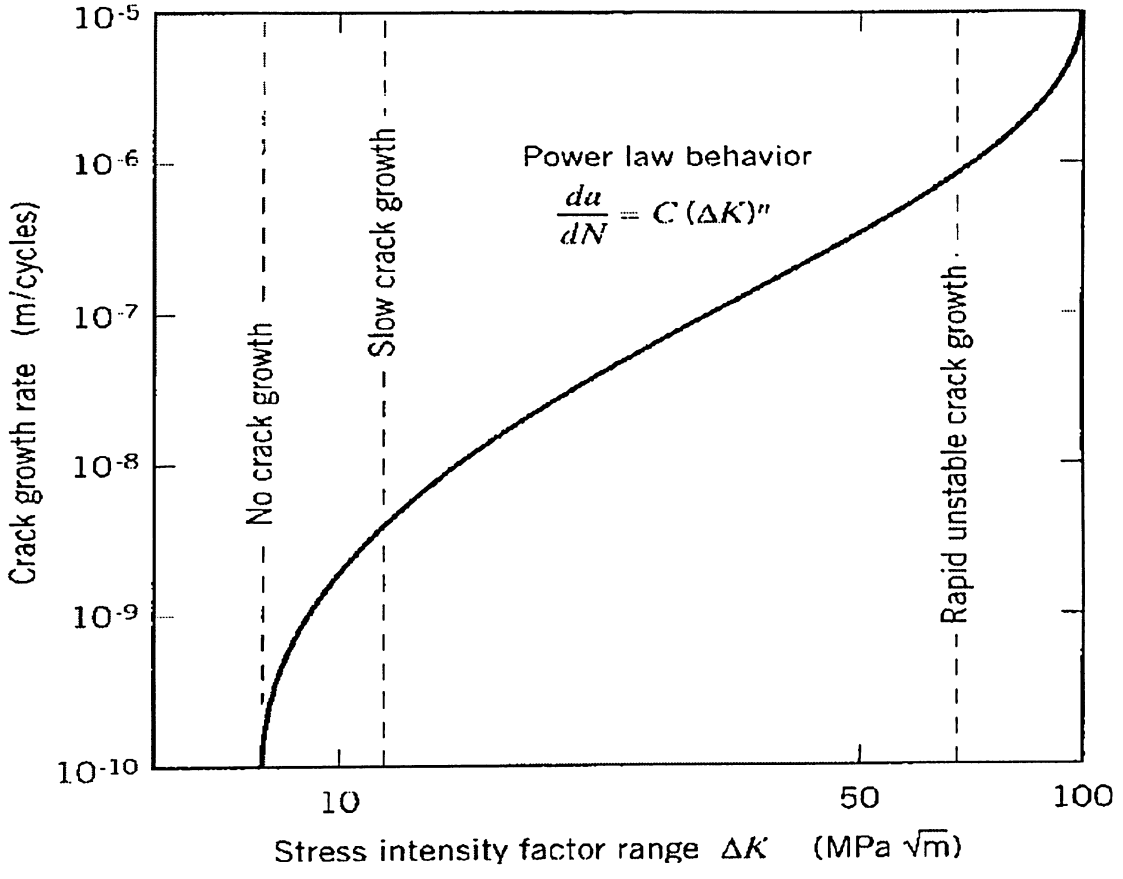

Fig. 8.1. The Paris law for fatigue crack growth rates

9. Strain – Life (ε - N) Approach

Three primary fatigue analysis methods are usually known as: (i) Strain-life (ε-N) method, (ii) Stress-life (S-N) method, (iii) The fracture mechanics method [8].
These methods have their own region of application with some degree of overlap between them. In broad terms the biggest differences are outlined as follows:

- Strain-life (ε-N) method only accounts for initiation life and can not be used to predict propagation life [8, p.236]
- Stress-life (S-N) approach does not distinguish between initiation and propagation regions [8, p.235]
- The fracture mechanics is the only method that deals directly with the propagation of fatigue cracks. It has problems when used to deal with crack initiation. [8, p.237]

The strain-life method is based on the observation that in wing root joints the response of the material in critical locations (notches) is strain or deformation dependent. When load levels are low, stresses and strains are linearly related. Consequently, in this range load-controlled and strain-controlled test results are equivalent. At high load levels, in the low cycle fatigue (LCF) regime, the cyclic stress-strain response and the material behaviour are best modeled under strain-controlled conditions.

Early fatigue researches showed that damage is dependent on plastic deformation or strain. In the strain-life approach the plastic strain or deformation is directly measured and quantified. The stress-life approach does not account for plastic strain. At long lives, where plastic strain is negligible and stress and strain are easily related, the strain-life and stress-life approaches are essentially the same [8, p. 40].

Although wing root attachments are designed such that the nominal loads remain elastic, stress concentrations often cause plastic strains to develop in the vicinity of notches. Due to the constraint imposed by the elastically stressed material surrounding the plastic zone, deformation at the notch root is considered strain-controlled.

The strain-life method requires that the notch root stresses and strains be known. These may be determined by the following methods:

- Strain gage measurements
- Finite element analysis (FEA)
- Methods that relate local stresses and strains to nominal values (using fatigue stress concentration factor)

The third alternative which is used in this project is often the least time-consuming and least expensive method of determining the local stresses and strains at the notch root.

9.1. Stress – Strain Relationships

The total strain ε_t can be split into elastic and plastic components:

Linear Elastic Strain: that portion of the strain which is recovered upon unloading, ε_e.

Plastic Strain (Nonlinear): that portion of the strain which can not be recovered upon unloading, ε_p (see Fig. 9.1.1).

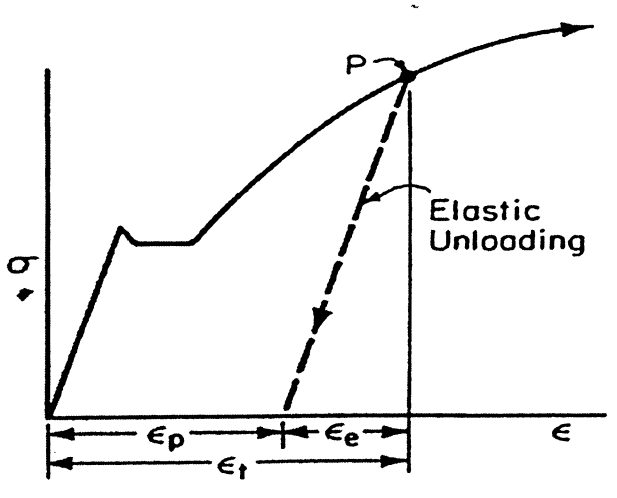

Fig. 9.1.1. Elastic and plastic strains

Stated in equation form, $\varepsilon_t = \varepsilon_e + \varepsilon_p$ Eq. 9.1.1

For most metals a log-log plot of true stress versus true plastic strain is modeled as a straight line. Consequently, this curve can be expressed using a power function:

$$\sigma = K(\varepsilon_p)^n \qquad \text{Eq. 9.1.2}$$

or $$\varepsilon_p = (\frac{\sigma}{K})^{\frac{1}{n}} \qquad \text{Eq. 9.1.3}$$

where K is the strength coefficient and n is the strain hardening exponent.

The elastic strain is defined as: $$\varepsilon_e = \frac{\sigma}{E} \qquad \text{Eq. 9.1.4}$$

The expression for plastic strain is given in Eq. 9.1.3. Equation 9.1.1 may then be re-written as:

$$\varepsilon_t = \frac{\sigma}{E} + (\frac{\sigma}{K})^{\frac{1}{n}} \qquad \text{Eq. 9.1.5}$$

9.2. Cyclic Stress – Strain Behavior

Monotonic stress-strain curves have long been used to obtain design parameters for limiting stresses on engineering structures subjected to static loading. Similarly, cyclic stress-strain curves are useful for assessing the durability of wing root joints which are subject to repeated loading.

The response of the joint subjected to cyclic in-elastic loading is in the form of a hysteresis loop, as shown in Fig. 9.2.1 and 9.2.2. $\Delta\varepsilon$ is the total width of the loop or the total strain range. $\Delta\sigma$ is the total height of the loop or the total stress range.

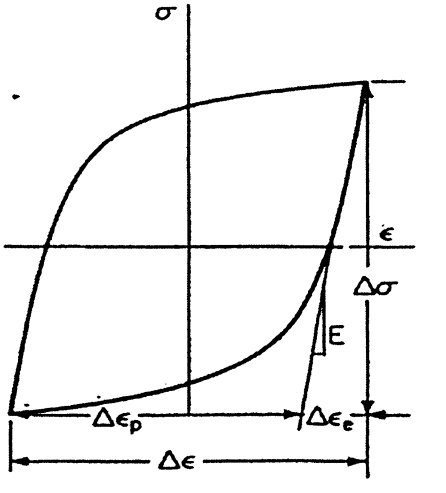

Fig. 9.2.1. Hysteresis loop

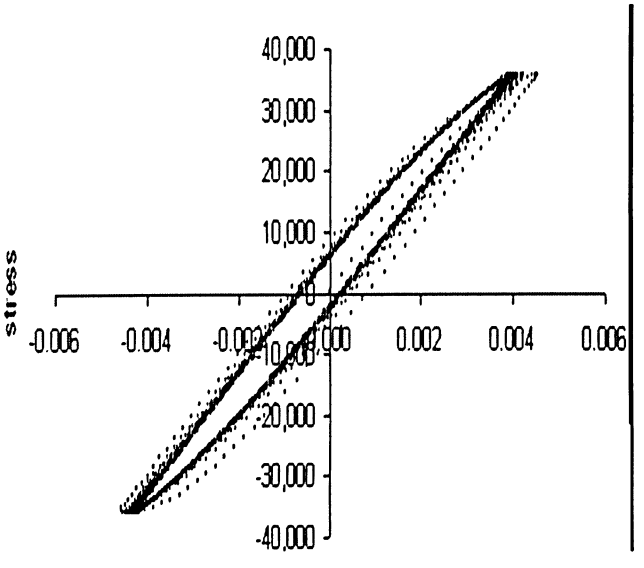

Fig. 9.2.2. Hysteresis loop data for 20 fatigue cycles [50]

These can be stated in terms of amplitudes: $\varepsilon_a = \frac{\Delta\varepsilon}{2}$

where ε_a is the strain amplitude and $\sigma_a = \frac{\Delta\sigma}{2}$

where σ_a is the stress amplitude. The total strain is the sum of the elastic and plastic strain ranges, $\Delta\varepsilon = \Delta\varepsilon_e + \Delta\varepsilon_p$ Eq. 9.2.1

or in terms of amplitudes, $\frac{\Delta\varepsilon}{2} = \frac{\Delta\varepsilon_e}{2} + \frac{\Delta\varepsilon_p}{2}$ Eq. 9.2.2

Using Hook's law, the elastic term may be replaced by $\Delta\sigma / E$.

$$\frac{\Delta\varepsilon}{2} = \frac{\Delta\sigma}{2E} + \frac{\Delta\varepsilon_p}{2} \quad \text{Eq. 9.2.3}$$

The area within the loop is the energy per unit volume dissipated during a cycle. It represents a measure of the plastic deformation work done on the material of the joint.

9.3. Low Cycle and High Cycle Fatigue

Low cycle fatigue (LCF) is the repeated cyclic loadings that cause significant plastic deformation (plastic straining) in a material and may cause fatigue cracking after a relatively small number of cycles; hundreds or thousands. So, LCF involves relatively short life. The analytical procedure used to address LCF or strain-controlled fatigue is commonly referred to as the Strain-Life, Crack-Initiation, or Critical Location approach.

Low cycle fatigue typically occurs as a result of repeated localized yielding near stress raisers, such as holes, fillets, and notches, despite the elastic deformation occurring over the bulk of a component such as wing root joint.

High cycle fatigue (HCF) is dominant where stresses and strains are largely confined to the elastic region. High-cycle fatigue is associated with low loads and long life. The Stress-Life (S-N) method is widely used for high-cycle fatigue applications. In this case the applied stress is within the elastic range and the number of cycles to failure is large. The dividing line between low and high cycle fatigue depends on the type of material which is used in wing root joint but 10^5 is a more referenced number.

10. Stress Concentration and Notch Effects on the Lug/Pin Attachment

The fracture of a wing root joint is dependent upon the forces that exist between the atoms. Because of the forces that exist between the atoms, there is a theoretical strength that is typically estimated to be one-tenth of the elastic modulus of the material of the joint. However, the experimentally measured fracture strengths of materials are found to be 10 to 1000 times below this theoretical value. The discrepancy is due to the presence of small flaws or cracks found either on the surface or within the material. These flaws cause the stress surrounding the flaw to be amplified where the magnification is dependent upon the orientation and geometry of the flaw. Shown in Fig. 10.1 is a stress profile across a cross section containing an internal, elliptically-shaped crack. The stress is at a maximum at the crack tip and decreased to the nominal applied stress with increasing distance away from the crack. The stress is concentrated around the crack tip or flaw developing the concept of *stress concentration*. *Stress raisers* are defined as the flaws having the ability to amplify an applied stress in the locale.

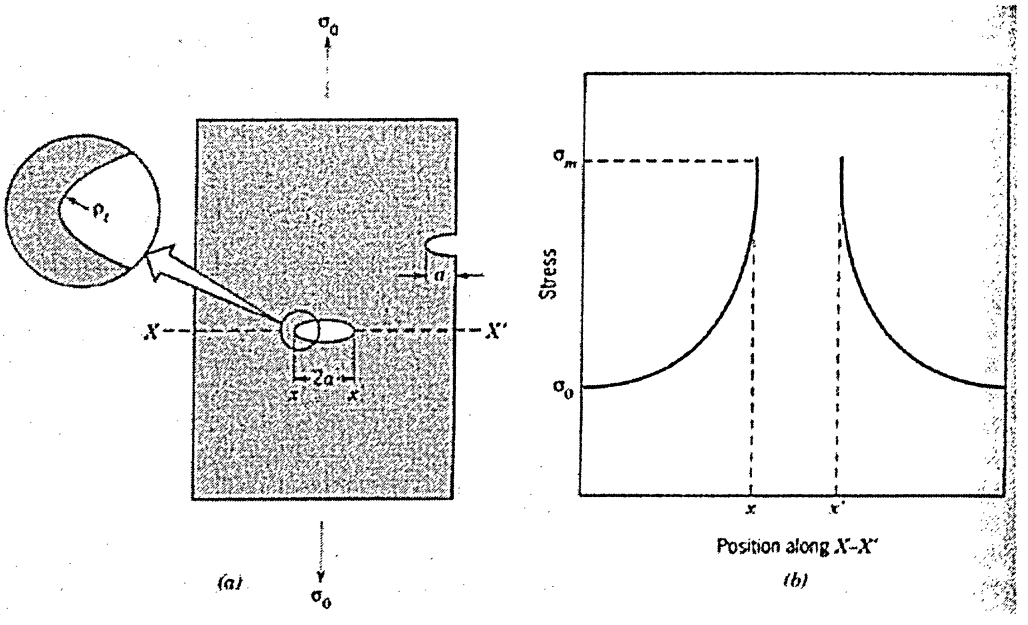

Fig. 10.1: (a) The geometry of surface and internal cracks. (b) Schematic stress profile along the axis X-X' (demonstrating stress amplification at crack tip positions) [49].

Wing root joints contain some form of geometrical or micro-structural discontinuities or changes in section and or shape. Common examples are shoulders on shafts, oil holes,

grooves, notches, press fits, key ways, screw threads, fillets, surface scratchs, sharp corners and bends. Metallurgical defects such as porosity, cavities, blow holes, slag, inclusions, decarburization and local overheating in grinding also work as stress raisers and have the same effect as that of a notch. Discontinuities in wing root joints are necessary for a number of purposes. For example in a lug/pin attachment holes are necessary to accommodate pins which transmit load between adjacent elements.

In practice, fatigue failure in a joint usually occurs at notches or stress concentrations. These discontinuities, or stress concentration factors, often result in maximum local stresses, σ_{max}, at the discontinuity that are many times greater than the nominal stress, σ, of the member.

Any discontinuity changes the stress distribution in the vicinity of the discontinuity, so that the basic stress analysis equations no longer apply. Such discontinuities or stress raisers cause local increase of stress referred to as stress concentration. Although wing root attachments are designed such that the nominal loads remain elastic, stress concentrations often cause plastic strains to develop in the vicinity of notches.

The uniform plate shown in the Fig.10.2 is subjected to a tensile load *P*. The stress σ in the plate is uniform everywhere with: $\sigma = P/W.T$

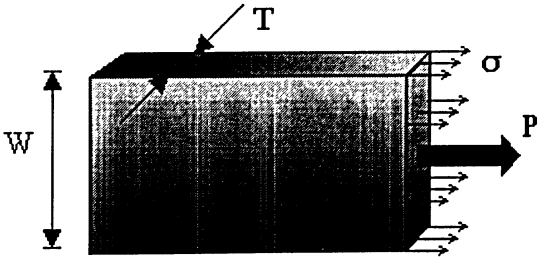

Fig. 10.2. A loaded uniform Plate

It is often necessary to drill a hole in plates (Fig.10.3). When the load *P* is applied, the presence of the hole disturbs the uniform stresses in the plate. Stress is increased 3 times.

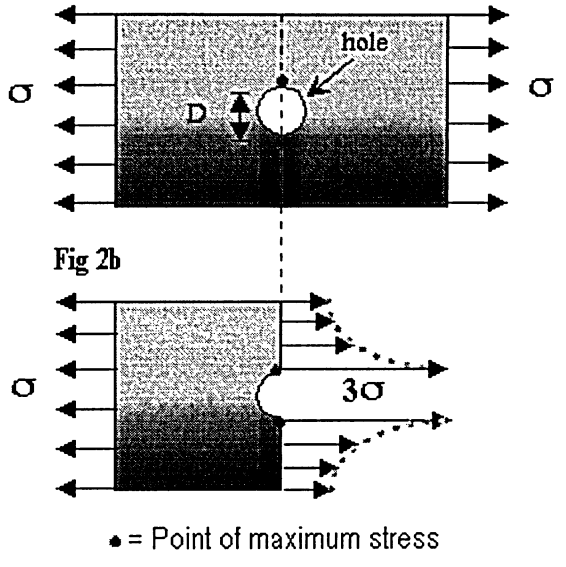

Fig.10.3. Stress distribution in presence of a discontinuity

Fig.10.1 and 10.3 are improved in Fig.10.4 to include stress distribution due to yielding that occurs at notch root of the joint. This indicates plastic deformation in the vicinity of a notch. Approximate shape of plastic zone around a notch root is shown in Fig. 10.5.

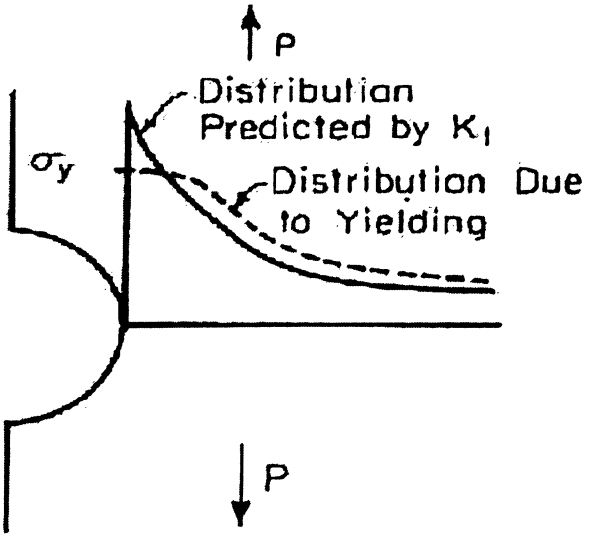

Fig.10.4. Comparison of stress distribution in presence of a notch. Horizontal part of the dotted curve represents plastic zone.

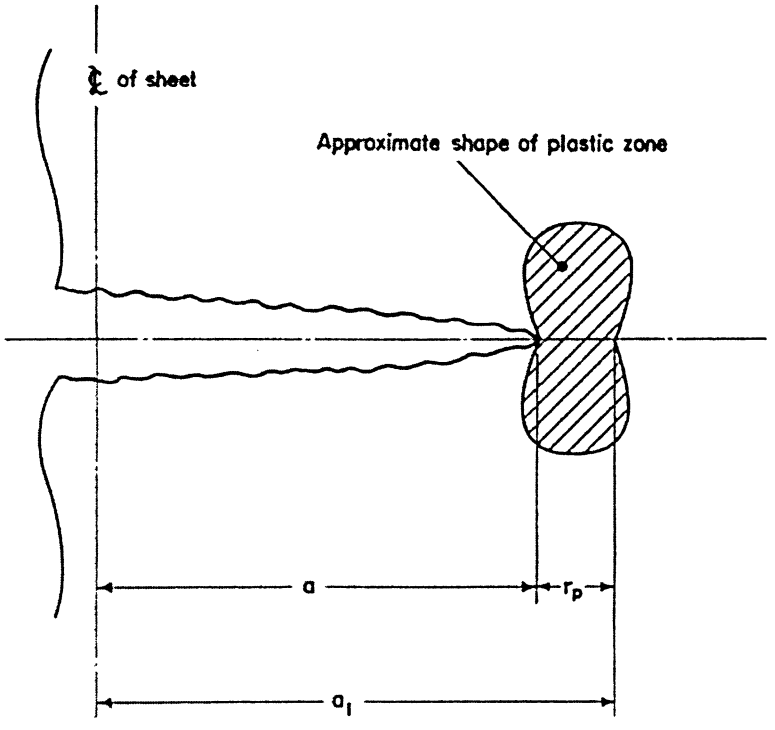

Fig.10.5. Approximate shape of plastic zone around a notch root

10.1. Notch Effects in wing root joints

A notch in a wing root joint under uniaxial loading results in:

- Stress concentration at the notch root;
- Stress gradient from the notch root toward the center of the wing root joint;
- Triaxial state of stress

The triaxial state of stress always exists at a notch. Triaxial stress state is a state of stress in which none of the three principal stresses is zero. This is when all the shear stresses (on the three orthogonal planes describing the material element) vanish, leaving only three (non-zero) normal stress components. Triaxial state of stress at notch root of a wing root joint is shown in Fig.10.1.1.

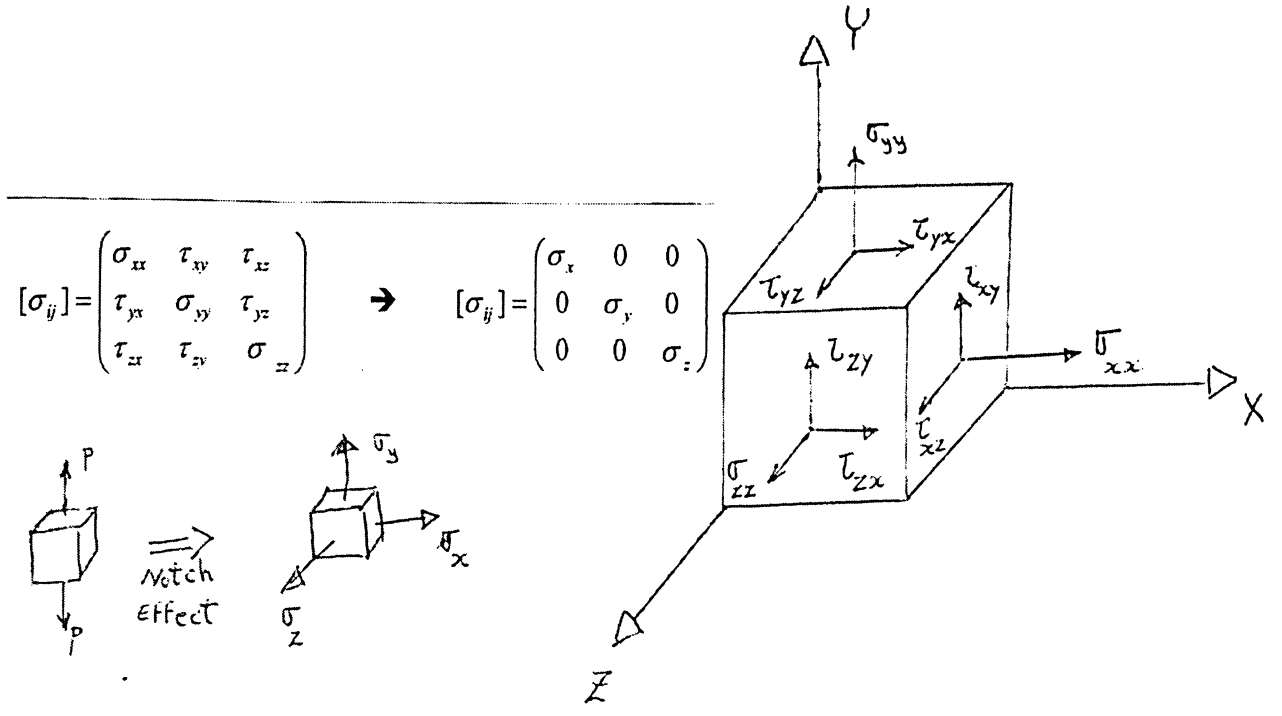

Fig.10.1.1. Triaxial state of stress at notch root of a wing root joint

A notch creates a local stress peak at the root of the notch. Plastic flow begins at the notch root when this local stress reaches the yield strength of the material used in the joint. The plastic flow relieves the high elastic stress and limits the peak stress to the yield stress of the material used in wing root joint. However, the most important effect of the notch is to produce a triaxial state of stress at the notch root rather than introducing a stress concentration and ultimately reducing the fatigue strength. The nominal (far field) strain may remain elastic in service, but the strains are often plastic in the notch roots. So, plastic deformation at the notch root is expected no matter what type of load is applied on wing root attachment.

The notch effect is illustrated using photoelasticity in Fig.10.1.2. Photoelasticity is an optical method for determining stresses in loaded components.

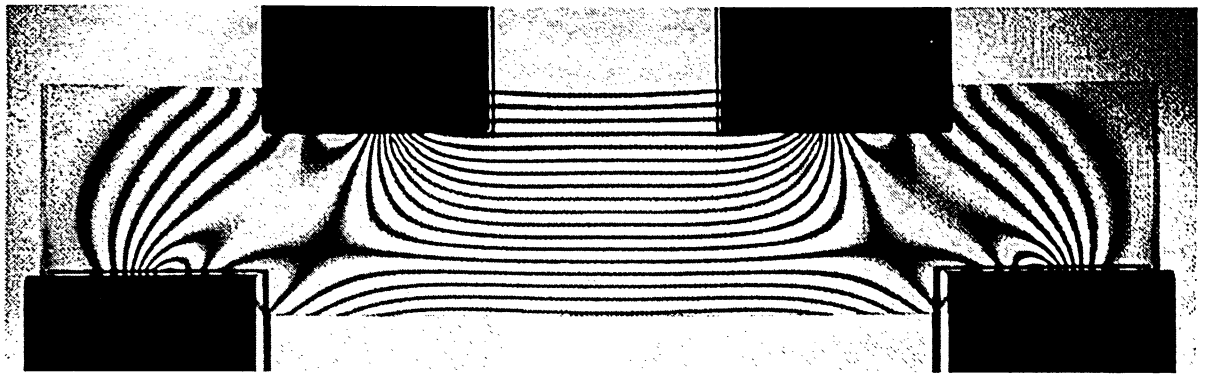

Fig. 10.1.2(a). Photoelastic fringe pattern of a uniform beam loaded in four-point bending. Contact rollers are hidden from view [25].

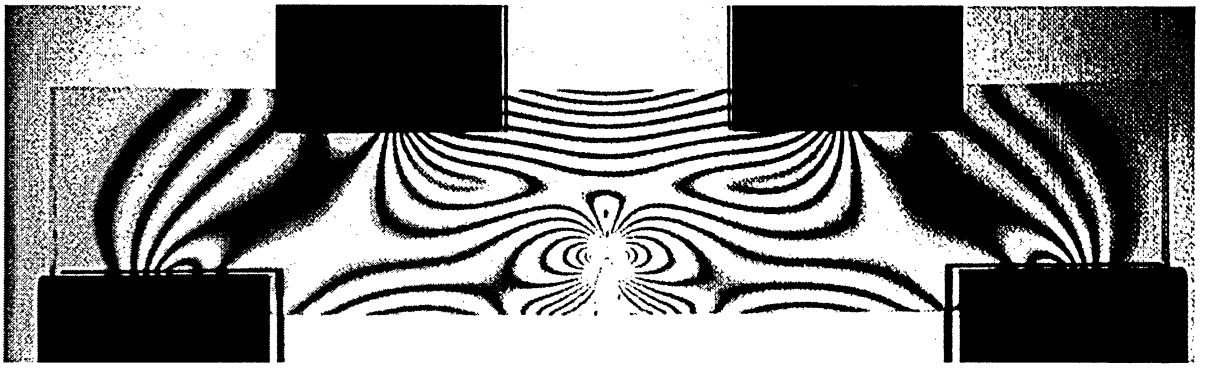

Fig. 10.1.2(b). Photoelastic fringe pattern of a sharp-notched beam loaded in four-point bending. Notch is loaded in tension [25].

Fig.10.1.3. illustrates a finite element model of one of the main wing root attachments used in a fighter jet [53]. One bolt hole and two fuel holes that are prone to fatigue cracks are shown in this figure. The edge of the fuel hole is identified as one of the critical areas in the wing attachment due to its high stress concentration. A fatigue experiment has been made for the crack growth at this area by introducing an initial crack of the size 1.27 mm with an aspect ratio of 1. The frame is then subjected to a simulated wing root load spectrum which is representative for corresponding fighter missions. Experimental fatigue crack growth results are shown in Fig. 10.1.4 as symbols [53].

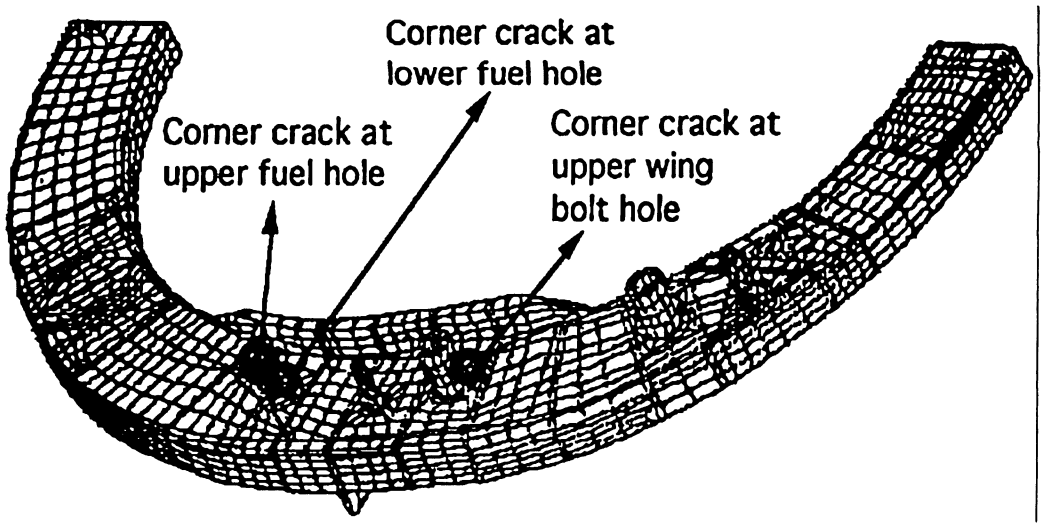

Fig. 10.1.3. Finite element model of the main wing attachment [53]

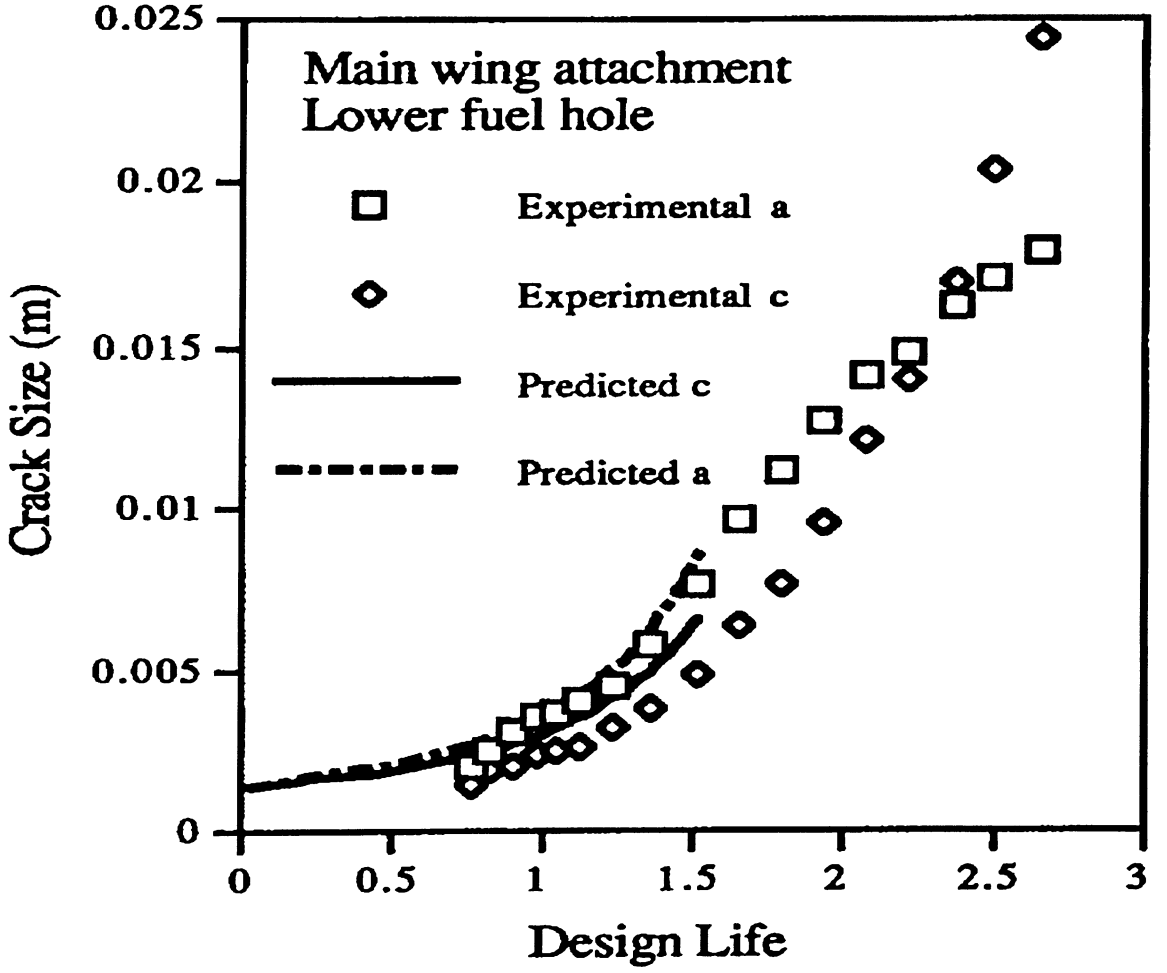

Fig. 10.1.4. Comparison of the predicted and experimental fatigue crack growth for a corner crack at the lower fuel hole in the main wing attachment, shown in Fig. 10.1.3 [53]

Fig. 10.1.5 depicts radial and hoop stress contours in a 2D and 3D finite element model for a wing lug attachment [54]. Stress concentrations that are prone to fatigue cracking are shown in red.

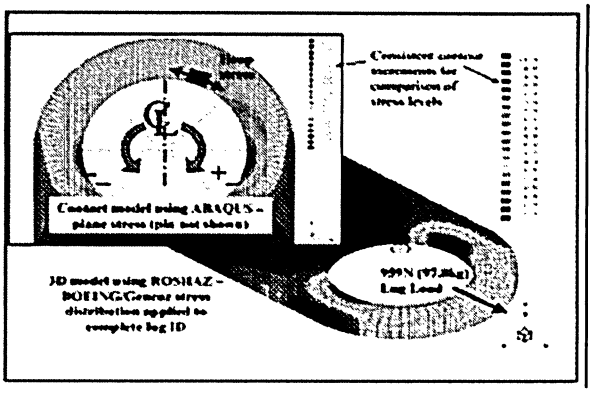

Fig. 10.1.5. Lug FEA model, radial and hoop stress contours - 2D and 3D [54]

10.2. Transfer of Stresses within Wing Root Joints

A wing root joint as a critical part of a wing must be designed such that it will accept all of the loads and stresses imposed on it by the flight and ground loads without any permanent deformation. Any repair made must accept the stresses, carry them across the repair, and then transfer them back into the original structure.

These stresses are considered as flowing through the structure; so, there must be a continuous path for them with no abrupt changes in cross-sectional areas along the way. Abrupt changes in cross-sectional areas of aircraft structure that are subject to cyclic loading / stresses will result in stress concentration that can potentially induce fatigue cracking and eventual failure. A scratch, notch or gouge in the surface of a highly-stressed piece of metal such as a wing root joint will cause a stress concentration at the point of damage.

11. Fatigue Damage

Fatigue damage is one of the most frequent forms of failure of metallic and non-metallic structures. With the increasing demand for high performance structures, the fatigue damage has become more and more important, in particular for metallic structures subjected to complex multiaxial loads (such as wing root joints) due to random vibrations and LCO. Fatigue damage limits the service life of wing root joints that are subject to variable stresses. Fatigue is irreversible and usually unavoidable. High priority objectives for preventing fatigue include containment of the fatigue damage, diagnostic tools to detect the beginning of fatigue damage, monitoring the damage evolution during service, prognostics for reliable prediction of remaining service life, and specifying fatigue-resistant materials by design.

Fatigue damage can result from fluctuating stresses. At low stress levels, the wing root joint behaves elastically and reversibly. However, if the stress is greater than the yield point, then irreversible plastic deformation occurs. If a single peak stress is high enough, fracture or other monotonic failures occur. If the stress is variable, so that there is a peak stress and an amplitude, then damage can accumulate with each cycle if the stress level is higher than S_e (endurance limit). After a sufficient number of cycles, failure can occur even if the peak stress is too low to cause fracture.

Fatigue is the leading cause of premature failure of wing root joints. Sometimes these failures can be quite catastrophic, leading to severe property damage and loss of life. Fatigue cracks can nucleate at pre-existing flaws in materials and tend to occur at stress concentrators in components such as notches or holes. Generally, fatigue damage is unavoidable. Once formed, the propagation rate of a crack is strongly influenced by load history and environmental factors. Thus, the accurate prediction of fatigue life is a complex problem.

All metals are subject to fatigue damage when stressed and strained cyclically at sufficiently high amplitudes. Although many parameters and techniques have been devised to model fatigue damage, the simplest and most practical technique is the Palmgren-Miner hypothesis.

11.1. Miner's Law for Cumulative Damage

Of the several cumulative fatigue damage theories available, the one most widely used and best known is the linear model suggested by Palmgren and later independently by Miner.

The Palmgren-Miner hypothesis is that the fatigue damage incurred at a given stress level is proportional to the number of cycles applied at that stress level divided by the total number of cycles required to cause failure at the same level [5, p. 549]. This damage is usually referred to as cumulative damage ratio.

When the cyclic load level varies during the fatigue process, a cumulative damage model is often hypothesized. To illustrate, take the lifetime to be *N1* cycles at a stress level σ_1 and *N2* at σ_2. If damage is assumed to accumulate at a constant rate during fatigue and a number of cycles *n1* is applied at stress σ_1, where *n1* < *N1* as shown in Fig. 11.1.1, then the fraction of lifetime consumed will be *n1*=*N1*. To determine how many additional cycles the component will survive at stress σ_2, an additional fraction of life will be available such that the sum of the two fractions equals one:

$$\frac{n_1}{N_1} + \frac{n_2}{N_2} = 1$$

Absolute cycles and not log cycles are used here. Solving for the remaining cycles permissible at σ_2:

$$n_2 = N_2\left(1 - \frac{n_1}{N_1}\right)$$

The generalization of this approach is called Miner's Law, and can be written as:

$$\sum \frac{n_j}{N_j} = 1$$

where n_j is the number of cycles applied at a load corresponding to a lifetime of N_j.

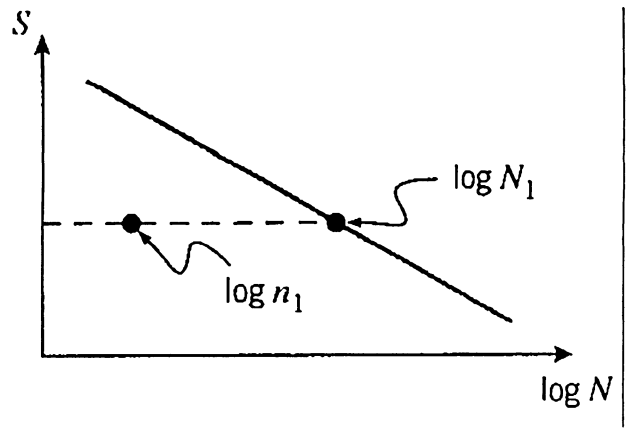

Fig. 11.1.1. The concept of fractional lifetime.

11.2. Nonlinear Models for Fatigue Damage

As stated earlier, Miner's rule is a linear damage model. This model is not comprehensive enough since it includes neither loading sequence nor material type. To overcome this deficiency many researches are conducted to include loading sequence, material type, stress amplitude and other influencing factors.

While many deviations from Miner's Rule have been observed and reported, and numerous modifications to this relationship have been proposed [19, pp 240-275], none has been proven better or gained wide acceptance.

Many nonlinear damage theories have been proposed which attempt to overcome the shortcomings of Miner's Rule. Among those Fatemi-Scocie and Varvani's models present the most comprehensive coverage. The author finds Varvani's model [51] superior since unlike many other nonlinear models it eliminates the need for using material-dependent coefficients.

Since nonlinear fatigue damage theories require other wide areas, and due to the fact that they are beyond the scope of this project work, they are not discussed in this report in detail.

12. Fatigue Behavior of the Lug/ Pin Attachment under LCO

12.1. Rainflow Stress Cycle Counting (ASTM E1049)

The Rainflow procedure is briefly introduced since it is frequently used in calculations for this project. Rainflow stress cycles counting invented by Matsuishi and Endo (1968) is the most common and practical form of stress cycle counting. Rainflow cycle counting is used to measure the impact of the most damaging stress cycles. It is only applicable for stress cycles in a single and constant direction (i.e. uniaxial loading). While theories have been advanced to extend the method to multiaxial loading, these are not generally accepted.

In the Rainflow method chronological information is discarded as they are irrelevant minor *noise* cycles. Gigabytes of raw stress data is reduced to Megabytes of good qualitative information. So the objective of the cycle counting is to reduce variable amplitude load history into constant amplitude events.

In addition, the Rainflow method is fairly easy to implement in computer code, most of which is derived from the original work of Downing and Socie in late 1970's [55].

A stress cycle is a closed loop in *load space* that can be completely defined by the amplitude and the mean-value. *Load space* is a two dimensional region with stress on one axis and strain on the other axis. Whenever a loop is closed, its amplitude and mean-value are determined, and the result recorded by incrementing a count in a bin of a two dimensional histogram of cycle amplitude versus mean-value.

The area within the stress loop represents an energy loss. The stored potential energy is not all returned. Some of this energy is absorbed by the crack forming process and remainder goes to heat generation.
Rainflow Counting refers to a various counting algorithms that reference closed hysteresis loops. Typical rules in this procedure are [8, p.190]:

1. To eliminate the counting of cycles, the strain-time history is drawn so as to begin and end at the strain value of greatest magnitude.

2. A flow of rain is begun at each strain reversal in the history and is allowed to continue to flow unless;
    a. The rain began at a local maximum point (peak) and falls opposite a local maximum point greater than that from which it came.
    b. The rain began at a local minimum point (valley) and falls opposite a local minimum point greater (in magnitude) than that from which it came.
    c. It encounters a previous rainflow.

12.2. Fatigue Behavior of the Lug/Pin Attachment under LCO

Some of the wing root joints incorporate lugs (female) and pins (male) in order to transfer load from one part to another. As discussed earlier the lug/pin attachment is widely adopted in aircraft wing designs for the following reasons:

- The lug/pin arrangement allows for good load transfer without excessive stress concentration,
- It also provides the freedom of movement required for deployment or actuation duties as required by any particular design,
- It is easy to assemble or remove,
- It is more economic for military fighters,
- It requires less manufacturing fitness,
- It has high structural efficiency and
- It has relatively low cost

Since lug/pin arrangements have some form of notch (e.g. holes), they are subject to plastic strain (deformation) at the notch root during cyclic loading. This permanent change in shape or size of a notch without fracture, produced by a sustained stress beyond the elastic limit of the material used in lug/pin, causes fatigue problems as per the mechanism discussed in Chapters 7 and 8. This means although design loads are maintained in the elastic region, holes of the lug/pin attachment experience plastic deformation, and subsequently, this is where fatigue cracking occurs.

The following five loadings are concerned about a lug/pin attachment of a fighter jet wing during LCO. In loading # 1, this wing root joint is subjected to a cyclic loading spectrum during LCO. Calculations indicate that loading # 1 is in the plastic region and the specified wing root joint has a short fatigue life (LCF).

The same lug/pin attachment then experiences various loading spectra to investigate the mean stress effect on fatigue life of the joint. The loading spectra are demonstrated in loading # 2 to loading # 5. Based on the calculations the specified wing root joint experiences plastic deformation. The calculations are given in the Appendix. It is shown that depending on the magnitude of the load spectrum this plastic deformation causes fatigue damage. Fatigue life is then estimated for the specified wing root joint in each loading. Loadings # 4 and 5 show elastic behaviour which imply infinite fatigue life for the lug/pin attachment.

Loading # 1, Plastic Region, Short Fatigue Life (LCF)

A lug/pin attachment of a fighter jet wing during LCO is subjected to a repeated bending stress spectrum as shown in Fig. 12.2.1. The load history shown in Fig. 12.2.1 is simulated. In practice, this kind of information can be obtained either by bonding strain gauges on the designated spots of the joint or it can be obtained by use of FEA for analytical determination. In the following five loadings the wing root joint is made up of a titanium alloy (Ti-6Al-4V) with the under mentioned material properties.

Material properties for a lug/pin attachment made up of Ti-6Al-4V are as follows:

Yield stress = $\sigma_y = 1{,}185 MPa$, Ultimate strength = $\sigma_u = 1{,}233 MPa$,

Fatigue strength coefficient = $\sigma_f' = 2{,}030 MPa$

Fatigue strength exponent = Slope of the elastic strain curve = b = -0.104

The fatigue life estimation technique for this specific wing root joint is given in the following.

Mean stress = $\sigma_m = \frac{\sigma_{max} + \sigma_{min}}{2}$, Alternating (amplitude) stress = $\sigma_a = \frac{\sigma_{max} - \sigma_{min}}{2}$

Goodman (1899) relationship [8, p. 7]: $\frac{\sigma_a}{S_e} + \frac{\sigma_m}{\sigma_u} = 1 \quad \Rightarrow$

$\Rightarrow S_e = \frac{\sigma_a}{1 - \frac{\sigma_m}{\sigma_u}}$ = Endurance limit = Fatigue strength = "Allowable stress [8, p. 24]"

True stress amplitude = $\frac{\Delta\sigma}{2} = \sigma'_f (2N_f)^b$ (Basquin's relationship [8, p. 59]). This equation can be re-written as: $N_{f.j.} = \frac{1}{2}(\frac{\sigma}{\sigma'_f})^{\frac{1}{b}}$ where $N_{f.j.}$ is fatigue life corresponding to stress cycle j. In this case S_e is used as σ because it is supposed to be allowable stress [8, p.24] (endurance limit or fatigue strength).

As shown in Fig.12.2.1, there are 3 stress cycles in this load history as per Rainflow procedure (ASTM E1049, described earlier). In practice, the number of stress cycles is usually determined by computer algorithms. There are 2 stress peaks, both 750 MPa, in the load history, so either one can be assumed as the starting point. In this illustration (Fig. 12.2.1) the left side stress peak has been chosen.

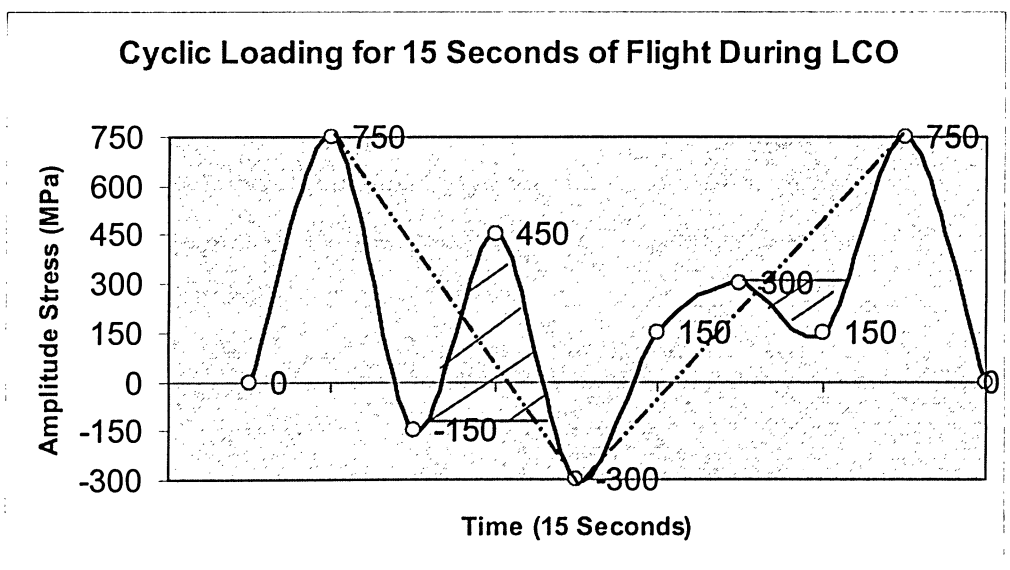

Fig. 12.2.1. Simulated cyclic bending stress history for a lug/pin arrangement of a fighter jet wing during 15 seconds of flight during LCO (Loading # 1). This load history is simulated. In practice, this kind of information can be obtained either by bonding strain gauges on the designated spots of the joint or it can be obtained by use of FEA for analytical determination.

Calculations have been summarized in Table 12.2.1.

j (Cycles)	n_j	$\sigma_{min}\,(MPa)$	$\sigma_{max}\,(MPa)$	σ_a	σ_m	S_e	$N_{f.j.}$
1	1	-150	450	300	150	341.5	$1.39x10^7$
2	1	150	300	75	225	91.7	$4.28x10^{12}$
3	1	-300	750	525	225	642.2	31,994

Table 12.2.1. Estimation of fatigue life for a lug/pin arrangement of a fighter jet wing (Loading # 1).

The number of fatigue cycles to failure can now be calculated by Palmgren-Miner's linear relationship (Chapter 11):

$$N_f, total = \frac{1}{\sum \frac{n_j}{N_{f.j}}} = \frac{1}{\sum Damage}$$

where n_j is the number of cycles applied at a load corresponding to a lifetime of N_j.

$$N_f, total = \frac{1}{\frac{1}{1.39x10^7} + \frac{1}{4.28x10^{12}} + \frac{1}{31,994}} = 31,920 \text{ cycles to failure.}$$

Since this figure is less than 100,000, it is referred to as low cycle fatigue (LCF).
Assuming the foregoing load history represents 15 seconds of a flight, then the life of this lug/pin joint can be estimated in terms of hours:

$$\text{N} = 31,920 \text{ cycles x } \frac{15}{3600} = 133 \text{ hours of flight}$$

As discussed earlier, the response of wing root joints, subjected to cyclic loading during LCO is in the form of a hysteresis loop illustrated in Fig. 12.2.2. $\Delta\varepsilon$ is the total width of the loop or the total strain range. $\Delta\sigma$ is the total height of the loop or the total stress range.

For the cyclic stress-strain curve shown in Fig. 12.2.2, $\sigma_{max} = 750$ MPa and $\varepsilon_{max} = 0.007547$.

The wing root joint is made up of a titanium alloy (Ti-6Al-4V) with the following material properties:

Fatigue ductility coefficient = $\varepsilon_f^{'} = 0.30$

Modulus of elasticity = E = 15.2 x 10^3 Ksi = 15.2 x 10^3 x 6.895 = 104,804 MPa

Fatigue ductility exponent = Slope of plastic strain curve = c = -0.6

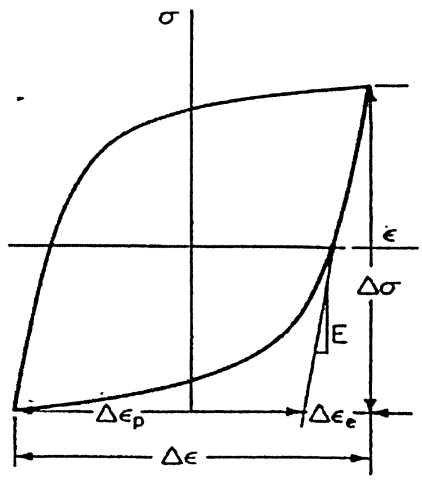

Fig. 12.2.2. Hysteresis loop for a lug/pin arrangement of a fighter jet wing subjected to cyclic loading

The fatigue life estimation technique for this specific wing root joint is given in the following. Coffin and Manson [8, p. 59] who were working independently in the 1950s, found that plastic strain-life (ε_p — N) data could be linearized on log-log coordinates. Plastic strain can be related by a power law function:

$$\frac{\Delta\varepsilon_p}{2} = \varepsilon_f'(2N_f)^c$$

If $\Delta\varepsilon_p$ is calculated, then fatigue life will be known. $\Delta\varepsilon_p$ can be calculated from the following equations.

Hook's law can be employed in elastic region, hence:

Elastic strain range: $\Delta\varepsilon_e = \frac{\Delta\sigma}{E} = \frac{2(750)}{104{,}804} = 1.431 \times 10^{-2}$

Plastic strain range: $\Delta\varepsilon_{plastic} = \Delta\varepsilon_{total} - \Delta\varepsilon_{elastic}$ =2(0.007547)-0.01431= 7.84×10^{-4}

Coffin-Manson equation: $\frac{\Delta\varepsilon_p}{2} = \varepsilon_f'(2N_f)^c \quad \Rightarrow \frac{7.84x10^{-4}}{2} = 0.3(2N_f)^{-0.6}$

$\Rightarrow 2N_f = 64{,}031 \quad \Rightarrow N_f = 32{,}016$ Cycles to failure

Since this figure is less than 100,000, it is referred to as low cycle fatigue (LCF).

As discussed earlier, Strain-life (ε-N) method provides better coverage for estimating fatigue life of the wing root joint.

Loading #1 in the next sections (Loading # 2 to Loading #5) is extended to experiencing various loading spectra to estimate fatigue life of the same lug/pin arrangement with above mentioned material properties for titanium alloy Ti-6Al-4V.

Loading # 2, Plastic Region, Long Fatigue Life (HCF)

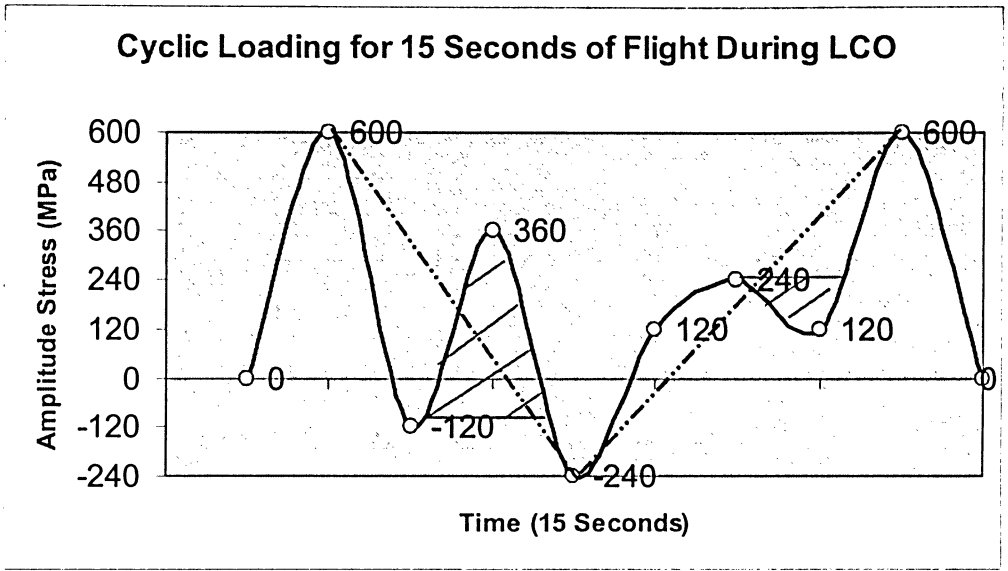

Fig. 12.2.3. Simulated cyclic bending stress history for a lug/pin arrangement of a fighter jet wing during 15 seconds of flight during LCO (Loading # 2).

Maximum stress in loading #2 is reduced down to 600 MPa. The interim calculations are given in the Appendix but the results are summarized in Table 12.2.3.

j (Cycles)	n_j	$\sigma_{min}\,(MPa)$	$\sigma_{max}\,(MPa)$	σ_a	σ_m	S_e	$N_{f.j.}$
1	1	-120	360	240	120	265.88	$1.54x10^8$
2	1	120	240	60	180	70.26	$5.56x10^{13}$
3	1	-240	600	420	180	491.79	416,177

Table 12.2.3. Estimation of fatigue life for a lug/pin arrangement of a fighter jet wing (Loading # 2).

$N_f, total = 415{,}055$ cycles to failure.

Since this figure is greater than 100,000, it is referred to as high cycle fatigue (HCF).

$$N = 415{,}055 \text{ cycles x } \frac{15}{3600} = 1{,}729.4 \text{ hours of flight}$$

Loading # 3, Plastic Region, Long Fatigue Life (HCF)

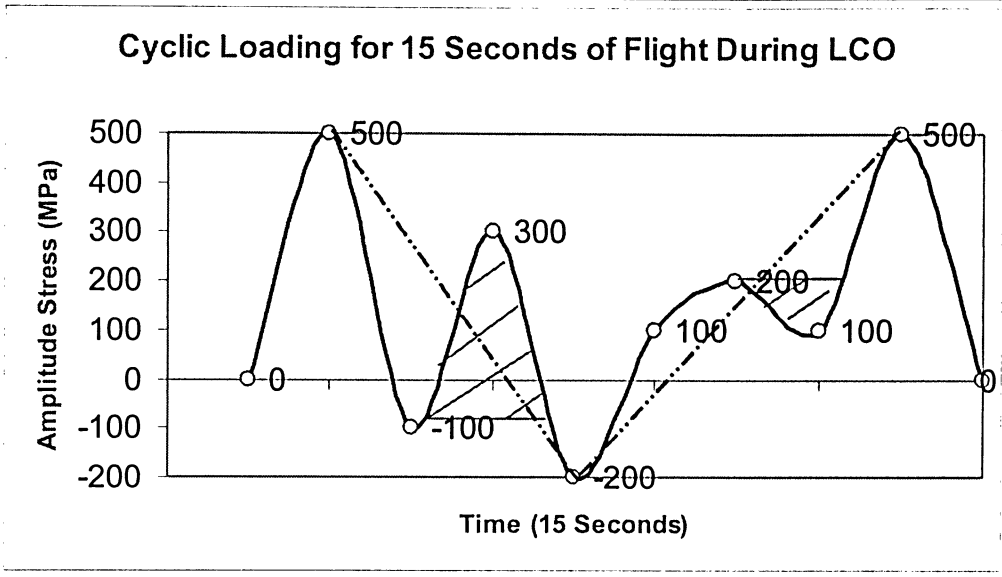

Fig. 12.2.4. Simulated cyclic bending stress history for a lug/pin arrangement of a fighter jet wing during 15 seconds of flight during LCO (Loading # 3).

Maximum stress in loading #3 is reduced down to 500 MPa. The interim calculations are given in the appendix but the results are summarized in Table 12.2.4.

j (Cycles)	n_j	$\sigma_{min}\,(MPa)$	$\sigma_{max}\,(MPa)$	σ_a	σ_m	S_e	$N_{f.j.}$
1	1	-100	300	200	100	217.65	$1.06x10^9$
2	1	100	200	50	150	56.93	$4.21x10^{14}$
3	1	-200	500	350	150	398.48	$3.15x10^6$

Table 12.2.4. Estimation of fatigue life for a lug/pin arrangement of a fighter jet wing (Loading # 3).

$N_f, total = 3.14x10^6$ cycles to failure.

Since this figure is greater than 100,000, it is referred to as high cycle fatigue (HCF).

$$N = 3.14x10^6 \text{ cycles x } \frac{15}{3600} = 13{,}083.3 \text{ hours of flight}$$

Loading # 4, Elastic Region, Infinite Fatigue Life

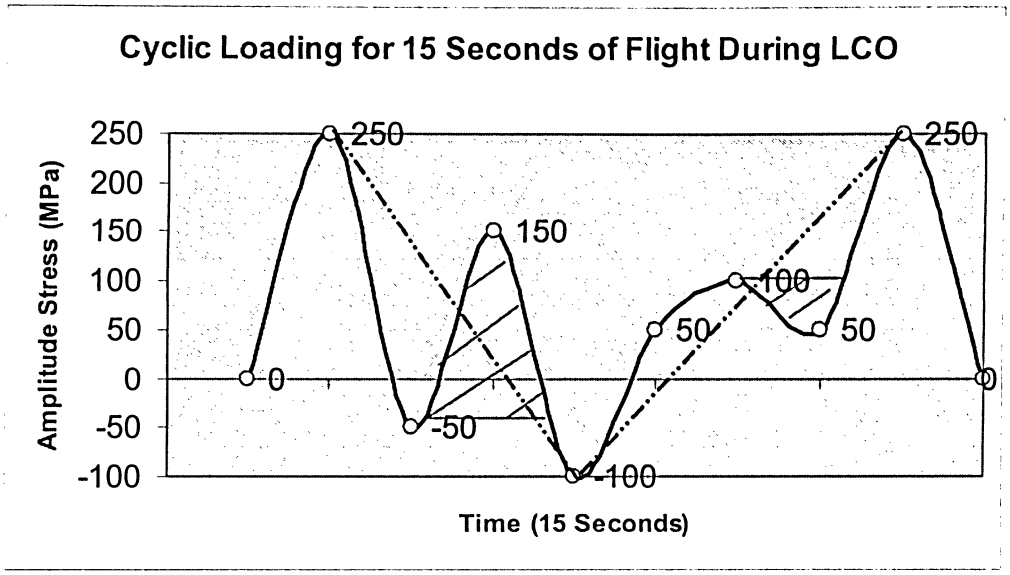

Fig. 12.2.5. Simulated cyclic bending stress history for a lug/pin arrangement of a fighter jet wing during 15 seconds of flight during LCO (Loading # 4).

Maximum stress in loading #4 is reduced down to 250 MPa. The interim calculations are given in the appendix but the results are summarized in Table 12.2.5.

j (Cycles)	n_j	$\sigma_{min}\,(MPa)$	$\sigma_{max}\,(MPa)$	σ_a	σ_m	S_e	$N_{f.j.}$
1	1	-50	150	100	50	104.23	$1.25x10^{12}$
2	1	50	100	25	75	26.62	$6.28x10^{17}$
3	1	-100	250	175	75	186.33	$4.7x10^{9}$

Table 12.2.5. Estimation of fatigue life for a lug/pin arrangement of a fighter jet wing (Loading # 4).

$N_f, total = 4.68x10^9$ cycles to failure.

N = $4.68x10^9$ cycles x $\frac{15}{3{,}600} = 1.95x10^7$ hours of flight which means infinite fatigue life which occurs in the elastic region.

Loading # 5, Elastic Region, Infinite Fatigue Life

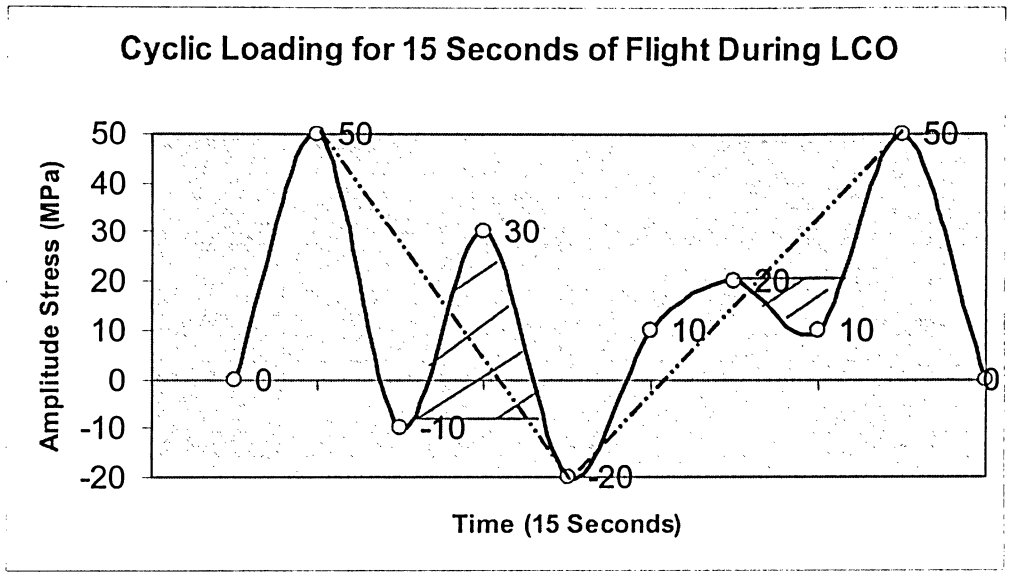

Fig. 12.2.6. Simulated cyclic bending stress history for a lug/pin arrangement of a fighter jet wing during 15 seconds of flight during LCO (Loading # 5).

Maximum stress in loading #5 is reduced down to 50 MPa. The interim calculations are given in the appendix but the results are summarized in Table 12.2.6.

j (Cycles)	n_j	$\sigma_{min}\,(MPa)$	$\sigma_{max}\,(MPa)$	σ_a	σ_m	S_e	$N_{f.j.}$
1	1	-10	30	20	10	20.16	$9.09x10^{18}$
2	1	10	20	5	15	5.06	$5.38x10^{24}$
3	1	-20	50	35	15	35.43	$4.02x10^{16}$

Table 12.2.6. Estimation of fatigue life for a lug/pin arrangement of a fighter jet wing (Loading # 5).

$N_f, total = 4.00x10^{16}$ cycles to failure.

$N = 4.00x10^{16}$ cycles x $\frac{15}{3{,}600} = 1.67x10^{14}$ hours of flight which means infinite fatigue life which occurs in the elastic region.

13. Strain – Life (ε , N) Curve for the Lug/Pin Attachment

In 1910, Basquin [8, p. 59] observed that stress-life (S-N) data could be plotted linearly on a log-log scale. Using the true stress amplitude, the plot may be linearized by:

$$\frac{\Delta\sigma}{2} = \sigma'_f (2N_f)^b \qquad \text{Eq. 13.1}$$

where $\frac{\Delta\sigma}{2}$ = true stress amplitude, $2N_f$ = reversals to failure (2 reversals = 1 cycle),

σ'_f = fatigue strength coefficient, b = fatigue strength exponent (Basquin's exponent)

σ'_f and b are fatigue properties of material of the joint.

Coffin- Manson equation [8, p. 59]:

$$\frac{\Delta\varepsilon_p}{2} = \varepsilon'_f (2N_f)^c \qquad \text{Eq. 13.2}$$

where $\frac{\Delta\varepsilon_p}{2}$ = plastic strain amplitude, $2N_f$ = reversals to failure, ε'_f = fatigue ductility coefficient and c = fatigue ductility exponent.

ε'_f and c are also fatigue properties of material of the joint.

An expression may now be developed that relates total strain range to fatigue life. In terms of strain amplitude,

$$\frac{\Delta\varepsilon}{2} = \frac{\Delta\varepsilon_e}{2} + \frac{\Delta\varepsilon_p}{2} \qquad \text{Eq. 13.3}$$

The elastic term can be written as: $\frac{\Delta\varepsilon_e}{2} = \frac{\Delta\sigma}{2E}$ Eq. 13.4

Using Eq. 13.1 this can be stated in terms of reversals to failure:

$$\frac{\Delta\varepsilon_e}{2} = \frac{\sigma'_f}{E}(2N_f)^b \qquad \text{Eq. 13.5}$$

Using Eq. 13.3, the total strain can now be re-written:

$$\frac{\Delta\varepsilon}{2} = \frac{\sigma'_f}{E}(2N_f)^b + \varepsilon'_f(2N_f)^c \qquad \text{Eq. 13.6}$$

elastic + plastic

Equation 13.6 can also be explained graphically. The elastic and plastic relations are both straight lines on a log-log plot, the total strain amplitude, $\Delta\varepsilon/2$, can be plotted simply by summing the elastic and plastic values as shown in Fig. 13.1. At large strain amplitudes the strain-life curve approaches the plastic line, and at low amplitudes, the curve approaches the elastic line.

In Fig. 13.1., the transition fatigue life, N_t, represents the life at which the elastic and plastic curves intersect. This is the life at which the stabilized hysteresis loop has equal elastic and plastic strain components. By equating elastic and plastic terms the following expression is derived for the transition life:

$$\frac{\Delta\varepsilon_e}{2} = \frac{\Delta\varepsilon_p}{2}$$

$$\frac{\sigma'_f}{E}(2N_f)^b = \varepsilon'_f(2N_f)^c \qquad \text{at } N_f = N_t$$

$$2N_t = \left(\frac{\varepsilon'_f . E}{\sigma'_f}\right)^{\frac{1}{b-c}} \qquad \text{Eq. 13.8}$$

A schematic representation of the shape of the hysteresis loop at different lives is shown in Fig. 13.1 in relationship to the transition life. As seen, at shorter lives more plastic strain is present and the loop is wider. At long lives the loop is narrower, representing less plastic strain.

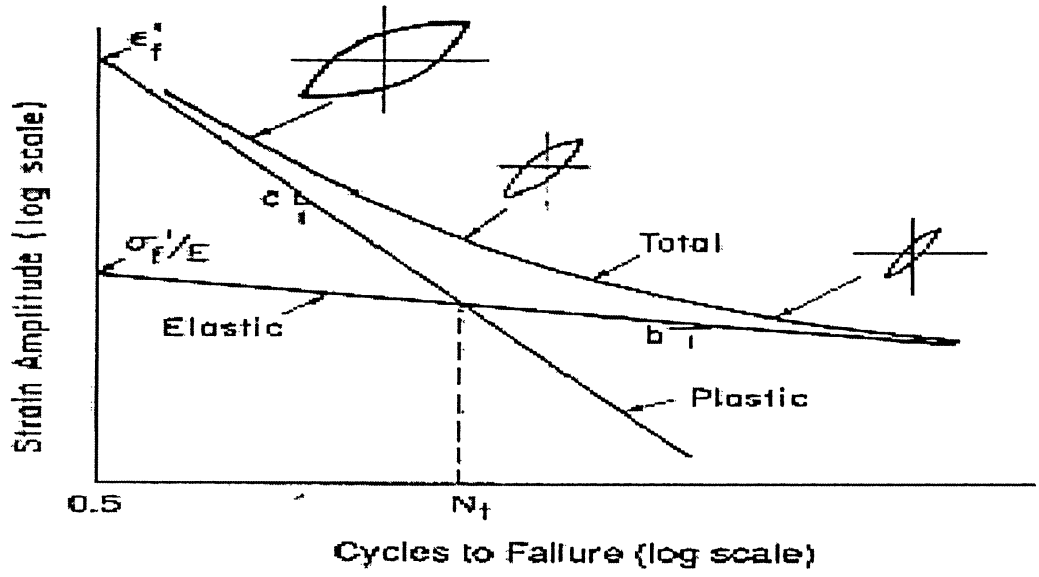

Fig. 13.1. Strain-life curve [6, p. 393]

Strain-Life (ε - N) curve for specified lug/pin attachment is calculated and plotted (in Fig. 13.2) as follows:

$$2N_t = \left(\frac{0.3x104{,}804}{2{,}030}\right)^{\frac{1}{-0.104+0.6}} = 250.7 \quad \text{reversals}$$

Since transition fatigue life, $2N_t$ is the life at which the stabilized hysteresis loop has equal elastic and plastic strain components, then:

$$\frac{\sigma_f'}{E}(2N_f)^b = \varepsilon_f'(2N_f)^c \qquad \text{at } N_f = N_t$$

$$\frac{\sigma_f'}{E}(2N_f)^b = \frac{2{,}030}{104{,}804}(250.7)^{-0.104} = 0.010904 = \varepsilon_e = \text{Elastic strain}$$

Now the stress level at which elastic and plastic strain components are equal can be calculated by Hook's law:

$\sigma = E.\varepsilon_e$=104,804 x 0.010904=1,142.82 MPa

It is evident that this stress is lower than yield stress (σ_y=1,185 MPa). Now strain-life curve can be plotted for the lug/pin attachment with the following information:

$\frac{\sigma'_f}{E} = \frac{2{,}030}{104{,}804}$=0.02 ; ε'_f = 0.30 (on Y-axis) and $2N_t$=251 (on X-axis, see Fig. 13.2)

Slope of the elastic strain curve = b = -0.104 = Fatigue strength exponent

Slope of the plastic strain curve = c = -0.6 = Fatigue ductility exponent (see Fig. 13.2)

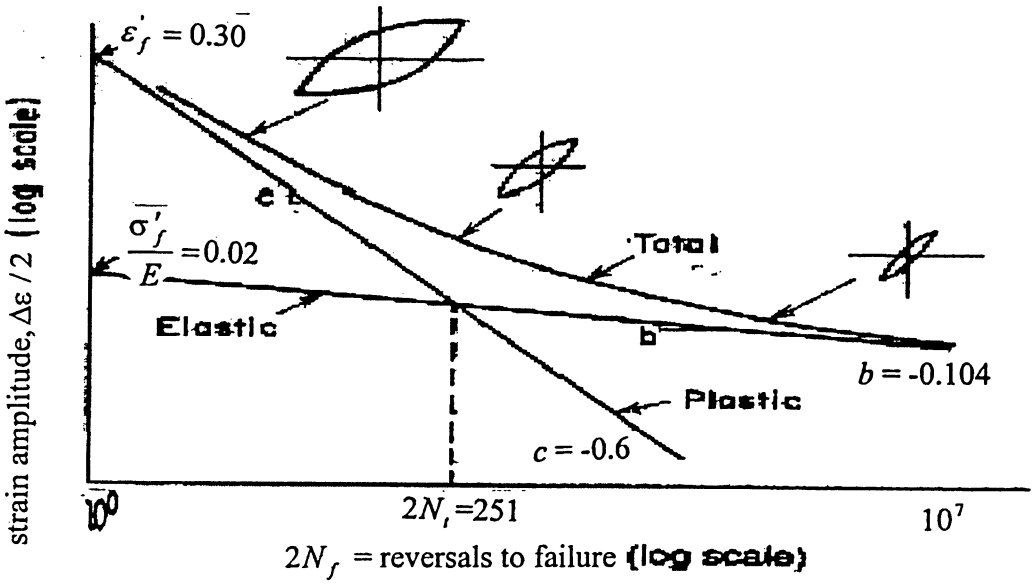

Fig. 13.2. Strain-life curve for the lug/pin arrangement of a fighter jet wing

14. Mean Stress Effects on Fatigue Life of the Lug/Pin Attachment

When a cyclic load is fully reversed mean stress is zero. Wing root joints seldom experience fully reversed loading, as some mean stress or mean strain is usually present. The effect of mean strain is negligible on the fatigue life of a wing root joint [8, p.67]. Mean stresses, on the other hand, may have a significant effect on the fatigue life.

Mean stresses can either increase the fatigue life with a nominally compressive load or decrease it with a nominally tensile value, as shown schematically in Fig. 14.1.

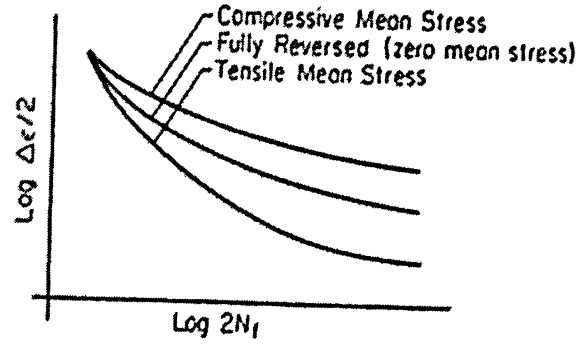

Fig. 14.1. Effect of mean stress on strain-life curve [8, p. 67]

Loadings # 1 to 5 (Chapter 12) are extended to experience constant amplitude of loadings to investigate the mean stress effect on fatigue life of the lug/pin attachment.

Loading # 1.1, Plastic Region, Short Fatigue Life (LCF)

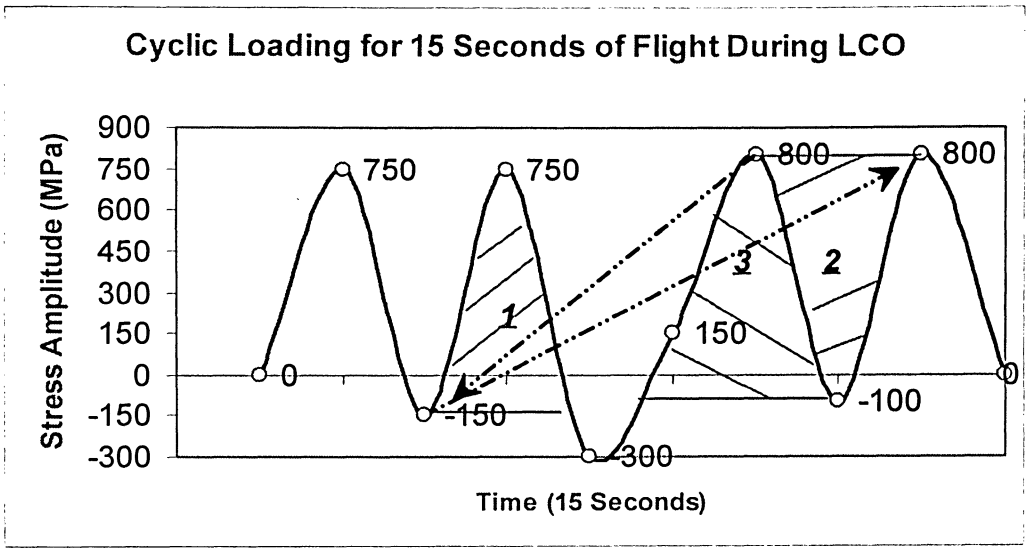

Fig. 14.2. Simulated cyclic bending stress history for a lug/pin arrangement of a fighter jet wing during 15 seconds of flight during LCO (Loading # 1.1).

Amplitude stresses (σ_a) in loading #1 (Chapter 12) are kept constant at 450 MPa in order to investigate the mean stress effect. The results of calculations are summarized in Table 14.2. During constant amplitude loading (constant σ_a), if σ_{max} is kept constant (Table 14.2- cycles 2 and 3), σ_{min} remains unchanged.

j (Cycles)	n_j	$\sigma_{min}(MPa)$	$\sigma_{max}(MPa)$	σ_a	σ_m	S_e	$N_{f.j.}$
1	1	-150	750	450	300	594.69	66,975
2	1	-100	800	450	350	628.37	39,437
3	1	-100	800	450	350	628.37	39,437

Table 14.2. Estimation of fatigue life for a lug/pin arrangement of a fighter jet wing (Loading # 1.1).

$N_f, total = 15{,}233.5$ cycles to failure.

Since this figure is less than 100,000 it is referred to as low cycle fatigue (LCF).

$$\text{N} = 15{,}233.5 \text{ cycles x } \frac{15}{3{,}600} = 63.5 \text{ hours of flight}$$

It is noted that fatigue life of the joint decreases as mean stress increases. Hence, the lower mean stress, the longer fatigue life.

Loading # 2.1, Plastic Region, Long Fatigue Life (HCF)

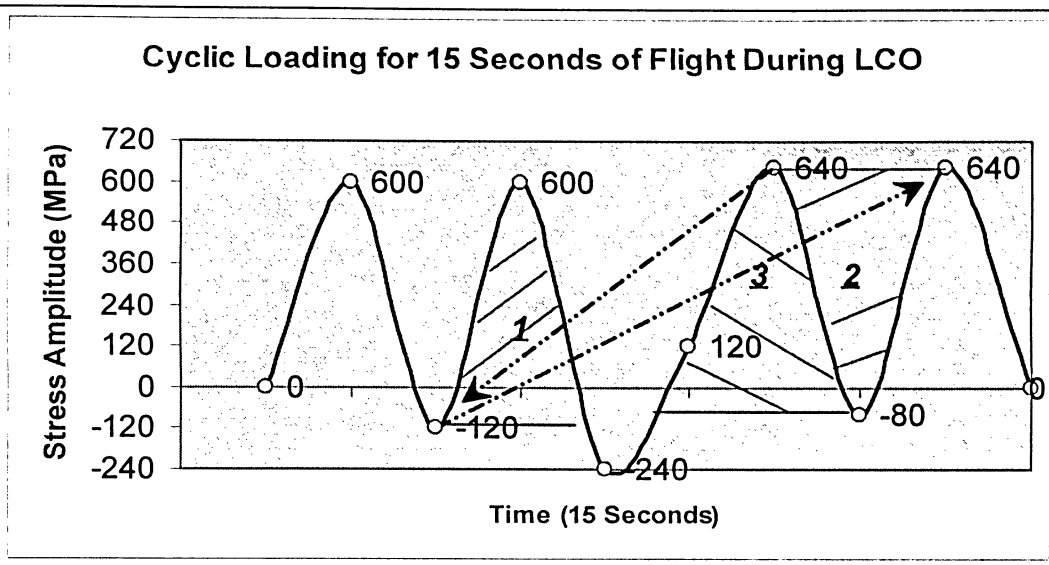

Fig. 14.3. Simulated cyclic bending stress history for a lug/pin arrangement of a fighter jet wing during 15 seconds of flight during LCO (Loading # 2.1).

Amplitude stresses (σ_a) in loading #2 (Chapter 12) are kept constant at 360 MPa in order to investigate mean stress effect. The results of calculations are summarized in Table 14.3. During constant amplitude loading (constant σ_a), if σ_{max} is kept constant (Table 14.3- cycles 2 and 3), σ_{min} remains unchanged.

j (Cycles)	n_j	$\sigma_{min}\,(MPa)$	$\sigma_{max}\,(MPa)$	σ_a	σ_m	S_e	$N_{f.j.}$
1	1	-120	600	360	240	447.01	$1.04x10^6$
2	1	-80	640	360	280	465.77	701,956
3	1	-80	640	360	280	465.77	701,956

Table 14.3. Estimation of fatigue life for a lug/pin arrangement of a fighter jet wing (Loading # 2.1).

$N_f, total = 262{,}565.8$ cycles to failure.

Since this figure is greater than 100,000 it is referred to as high cycle fatigue (HCF).

$$N = 262{,}565.8 \text{ cycles x } \frac{15}{3{,}600} = 1{,}094 \text{ hours of flight}$$

It is noted that fatigue life of the joint decreases as mean stress increases. Hence, the lower mean stress, the longer fatigue life.

Loading # 3.1, Plastic Region, Long Fatigue Life (HCF)

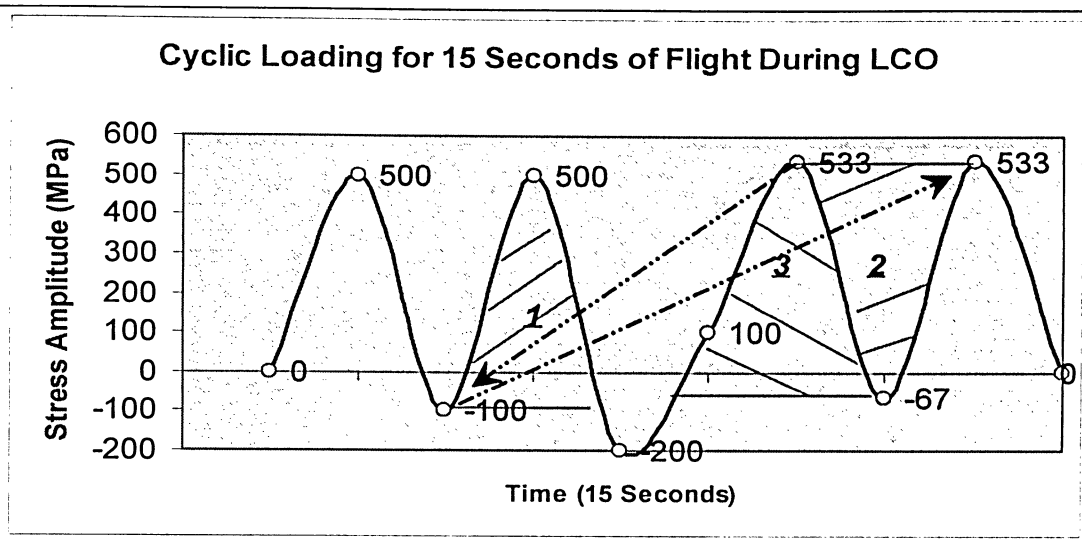

Fig. 14.4. Simulated cyclic bending stress history for a lug/pin arrangement of a fighter jet wing during 15 seconds of flight during LCO (Loading # 3.1).

Amplitude stresses (σ_a) in loading #3 (Chapter 12) are kept constant at 300 MPa in order to investigate mean stress effect. The results of calculations are summarized in Table 14.4. During constant amplitude loading (constant σ_a), if σ_{max} is kept constant (Table 14.4- cycles 2 and 3), σ_{min} remains unchanged.

j (Cycles)	n_j	$\sigma_{min}\,(MPa)$	$\sigma_{max}\,(MPa)$	σ_a	σ_m	S_e	$N_{f.j.}$
1	1	-100	500	300	200	358.08	$8.80x10^6$
2	1	-67	533	300	233	369.90	$6.44x10^6$
3	1	-67	533	300	233	369.90	$6.44x10^6$

Table 14.4. Estimation of fatigue life for a lug/pin arrangement of a fighter jet wing (Loading # 3.1).

$N_f, total = 2.36x10^6$ cycles to failure.

Since this figure is greater than 100,000 it is referred to as high cycle fatigue (HCF).

$$N = 2.36x10^6 \text{ cycles x } \frac{15}{3{,}600} = 9{,}818 \text{ hours of flight}$$

It is noted that fatigue life of the joint decreases as mean stress increases. Hence, the lower mean stress, the longer fatigue life.

Loading # 4.1, Elastic Region, Infinite Fatigue Life

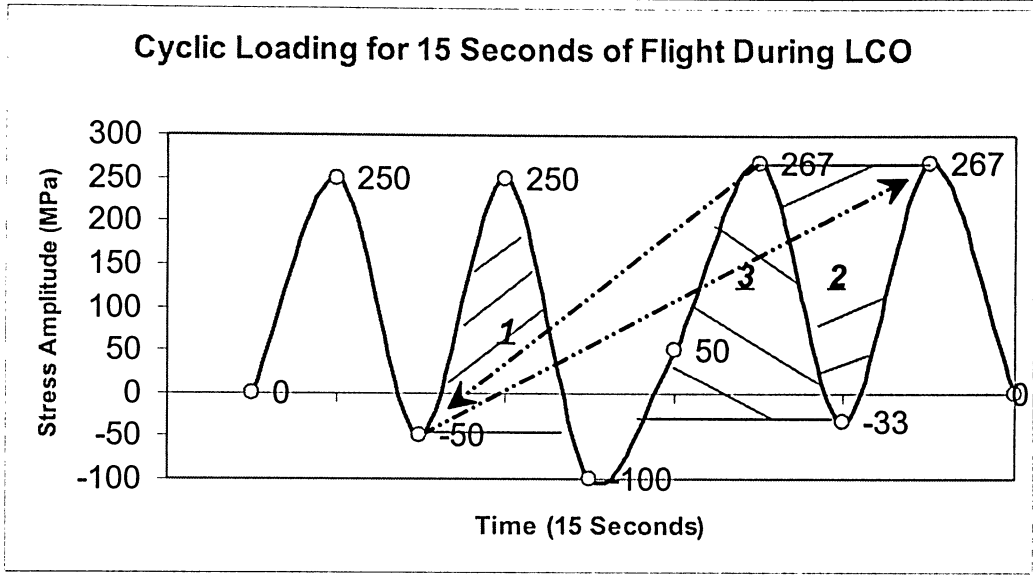

Fig. 14.5. Simulated cyclic bending stress history for a lug/pin arrangement of a fighter jet wing during 15 seconds of flight during LCO (Loading # 4.1).

Amplitude stresses (σ_a) in loading #4 (Chapter 12) are kept constant at 150 MPa in order to investigate mean stress effect. The results of calculations are summarized in Table 14.5. During constant amplitude loading (constant σ_a), if σ_{max} is kept constant (Table 14.5- cycles 2 and 3), σ_{min} remains unchanged.

j (Cycles)	n_j	$\sigma_{min}\,(MPa)$	$\sigma_{max}\,(MPa)$	σ_a	σ_m	S_e	$N_{f.j.}$
1	1	-50	250	150	100	163.24	$1.68x10^{10}$
2	1	-33	267	150	117	165.73	$1.45x10^{10}$
3	1	-33	267	150	117	165.73	$1.45x10^{10}$

Table 14.5. Estimation of fatigue life for a lug/pin arrangement of a fighter jet wing (Loading # 4.1).

$N_f, total = 5.06x10^9$ cycles to failure.

$$\text{N} = 5.06x10^9 \text{ cycles x } \frac{15}{3{,}600} = 2.11x10^7 \text{ hours of flight}$$

It is noted that fatigue life of the joint decreases as mean stress increases. Hence, the lower mean stress, the longer fatigue life.

Loading # 5.1, Elastic Region, Infinite Fatigue Life

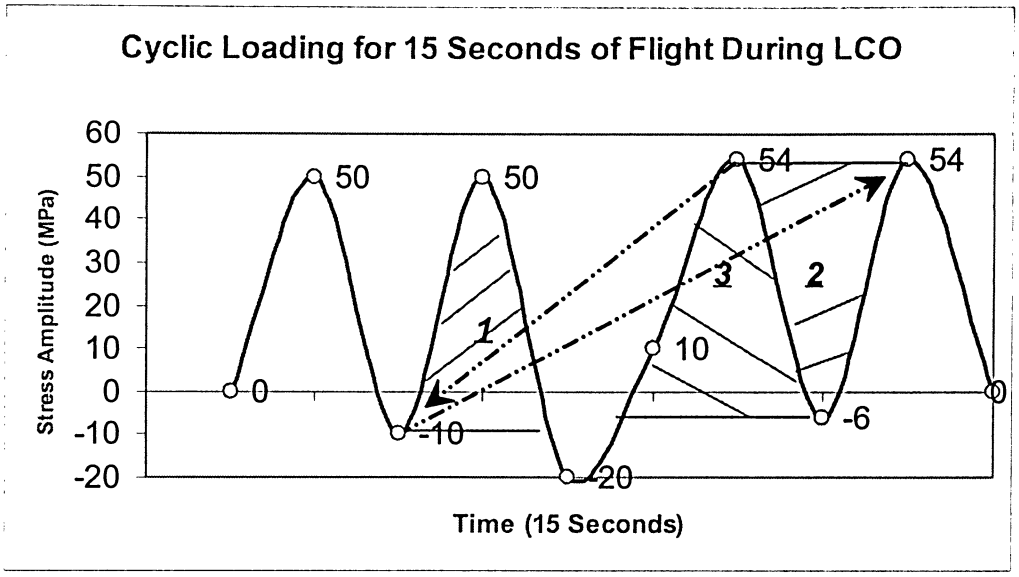

Fig. 14.6. Simulated cyclic bending stress history for a lug/pin arrangement of a fighter jet wing during 15 seconds of flight during LCO (Loading # 5.1).

Amplitude stresses (σ_a) in loading #5 (Chapter 12) are kept constant at 30 MPa in order to investigate mean stress effect. The results of calculations are summarized in Table 14.6. During constant amplitude loading (constant σ_a), if σ_{max} is kept constant (Table 14.6- cycles 2 and 3), σ_{min} remains unchanged.

j (Cycles)	n_j	$\sigma_{min}(MPa)$	$\sigma_{max}(MPa)$	σ_a	σ_m	S_e	$N_{f.j.}$
1	1	-10	50	30	20	30.49	$1.70x10^{17}$
2	1	-6	54	30	24	30.60	$1.65x10^{17}$
3	1	-6	54	30	24	30.60	$1.65x10^{17}$

Table 14.6. Estimation of fatigue life for a lug/pin arrangement of a fighter jet wing (Loading # 5.1).

$N_f, total = 5.55x10^{16}$ cycles to failure.

$$N = 5.55x10^{16} \text{ cycles x } \frac{15}{3{,}600} = 2.31x10^{14} \text{ hours of flight}$$

It is noted that fatigue life of the joint decreases as mean stress increases. Hence, the lower mean stress, the longer fatigue life.

14.1. Compressive Mean Stress Effect on life of the Lug/Pin Attachment

Loading # 6.1 (Fig. 14.1.1) illustrates the effect of compressive mean stress on life of the lug/pin arrangement.

Loading # 6.1, Effect of Compressive Mean Stress

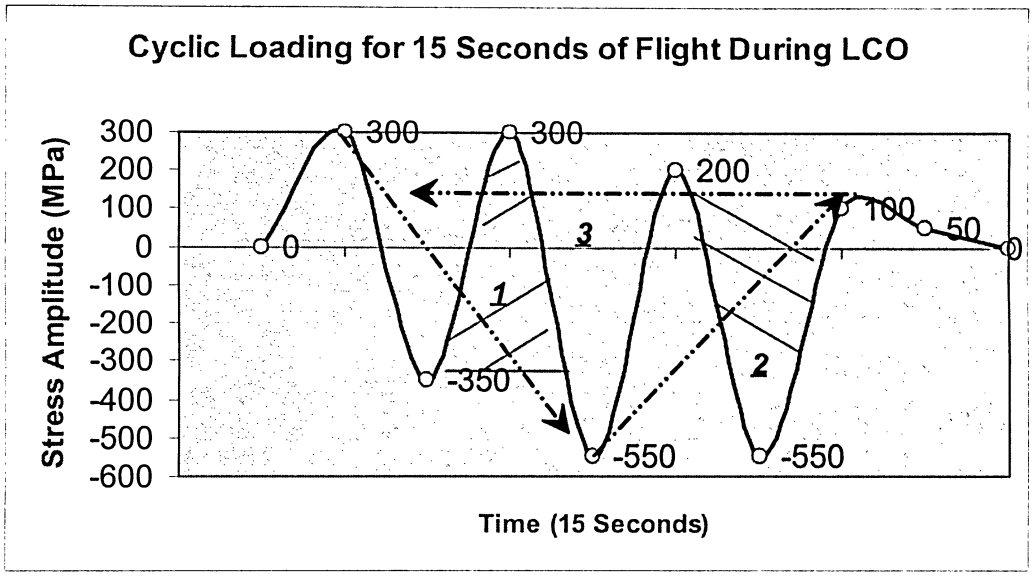

Fig. 14.1.1. Simulated cyclic bending stress history for a lug/pin arrangement of a fighter jet wing during 15 seconds of flight during LCO (Loading # 6.1).

The results of calculations are summarized in Table 14.1.1. During constant amplitude loading (constant σ_a), if σ_{max} is kept constant (Table 14.1.1- cycles 2 and 3), σ_{min} remains unchanged.

j (Cycles)	n_j	$\sigma_{min}\,(MPa)$	$\sigma_{max}\,(MPa)$	σ_a	σ_m	S_e	$N_{f.j.}$
1	1	-350	300	325	-25	318.54	$2.71x10^7$
2	1	-550	100	325	-225	274.85	$1.12x10^8$
3	1	-550	100	325	-225	274.85	$1.12x10^8$

Table 14.1.1. Estimation of fatigue life for a lug/pin arrangement of a fighter jet wing under compressive mean stress (Loading # 6.1)

$N_f, total = 1.83x10^7$ cycles to failure.

$$N = 1.83x10^7 \text{ cycles x } \frac{15}{3{,}600} = 76{,}076 \text{ hours of flight}$$

It is noted that fatigue life of the joint increases as mean stress decreases. Hence, compressive mean stress is beneficial to the fatigue life.

15. Conclusion and Future Work

15.1. Conclusion

The focus of this project was to investigate fatigue behavior of a titanium alloy wing root joint (Ti-6Al-4V) under various loading spectra during limit-cycle oscillations (LCO) by the strain-life ($\varepsilon - N$) approach. Although wing root attachments are designed such that the nominal loads remain elastic, stress concentrations often cause plastic strains to develop in the vicinity of notches and consequently wing loads caused by LCO, lead to fatigue damage accumulation. This project showed that:

- Cyclic loading during Limit-Cycle Oscillations can cause fatigue damage in wing root joints.
- Tensile mean stress is detrimental to the fatigue life of the wing root joint, while compressive mean stress is beneficial.

15.2. Future Work

Since the fatigue-LCO relationship is still in the early stages of research, it needs further investigations and analyses. Little is known or at least written about this cause-and-effect relationship in a flight vehicle. To the author's knowledge virtually nothing quantitative has been published in this regard.

As the first recommendation, future research work might be complemented by the following ingredients:

- Load sequence effects should be considered,
- Random overloads (e.g. gusty winds, etc) should be addressed,
- A non-linear fatigue damage model should be employed to provide more coverage,
- Then a fairly detailed finite element model should be developed and used in order to model an aircraft wing experiencing LCO,
- Depending on the scope of the research, an improvement on the explaining LCO-Fatigue cause-and-effect relationship should be accomplished, namely the effect of frequency,
- A mathematical model may also be developed to explain this cause and effect relationship quantitatively.

16. Bibliography

[1] "Gust loads on aircraft: Concepts and applications", F.M. Hoblit, AIAA Education series, 1988, ISBN 0-930403-45-2.

[2] "Fatigue in aircraft structures", Proceedings of the international conference, 1956, Edited by A.M. Freudenthal, Academic Press Inc.

[3] "Aircraft structures for engineering students", 2nd edition, T.H.G. Megson, 1990, ISBN: 0-7131-3681-2, Arnold Publishing Co.

[4] "Mixed mode fracture analysis of airframe materials", X. Deng, M.A. Sutton, J.Zuo, L.Wang, Aging Aircraft conference, 2001, USA

[5] "Airframe structural design", M.Chun-Yung Niu, Hong Kong Conmilit Press Ltd., 1995, ISBN: 962-7128-04-X

[6] "Mechanical Metallurgy",3rd edition, G.E. Dieter, McGraw-Hill, Boston, 1986

[7] "Metal fatigue in engineering", 2nd edition, R.I. Stephens, A. Fatemi, R.R. Stephens and H.O. Fuchs, John Wiley & Sons Inc. ,NY, 2001.

[8] "Fundamentals of metal fatigue analysis", J.A. Bannantine, J.J. Comer, J.L. Handrock, Prentice Hall, NJ, 1990.

[9] "Strength and fracture of engineering solids", 2nd edition, D.K. Felbeck, A.G. Atkins, Prentice Hall, NJ, 1996.

[10] "Deformation and fracture mechanics of engineering materials", 4th edition, R.W. Hertzberg, John Wiley & Sons, Inc. NY, 1996

[11] "Mechanical behaviour of materials", M.A. Meyers, K.K. Chawla, Prentice Hall, NJ, 1999.

[12] "Mechanical behaviour of materials", 2nd edition, N.E. Dowling, Prentice Hall, NJ, 1998.

[13] "The plastic deformation of metals", 2nd edition, R.W.K. Honeycombe, E. Arnold, London, 1984.

[14] "Fatigue of materials", 2nd edition, S. Suresh, Cambridge university press, 1998.

[15] "Fracture of brittle solids", 2nd edition, B. Lawn, Cambridge university press, 1993.

[16] "Principles of fracture mechanics", R.J. Sanford, Prentice Hall-Person education Inc., NJ, 2003.

[17] "Fatigue of metallic materials", 2nd edition, M. Klesnil, P. Lukas, Elsevier, Amsterdam, 1992.

[18] "Metal failures: Mechanisms, analysis, prevention", A.J. McEvily, John Wiley & Sons Inc. NY, 2002.

[19] "Failure of materials in mechanical design", J.A. Collins, John Wiley & Sons Inc. NY, 1993.

[20] "Analysis and Design of Flight Vehicle Structures", E. F. Brauhn, Jacobs Publishing, 1973

[21] "Strength of Materials", ISBN 0-486-60755-0, J. P. Den Hartog, 1949

[22] "SAE International, Technology update: All set for more wings", S. Birch, June 1999

[23] "Smoother Wing Leading-Edge Joints Would Favor Laminar Flow", Ames Research Center, Moffett Field, California, NASA Technical Briefs, June 1999

[24] "Biofilms", W.G. Characklis, K.C. Marshall, Wiley interscience publication, ISBN 0471826634, 1990

[25] "Experimental Stress Analysis", Dally, J. W., Riley, W. F., 3rd Edition., McGraw-Hill, Inc., New York, 1991

[26] "Probabilistic fracture prediction based on aircraft specific fatigue test data", P.White, S. Barter and L. Molent, 6th Joint FAA/DoD/NASA Aging Aircraft Conference proceedings, 2002

[27] "A comparison of the corrosion/ fatigue effects on sealed and unsealed longitudinal fuselage splices", M. Falugi, E. Tuegel, C. Brooks, R. Bell and D. Shelton, Aging Aircraft Conference proceedings, 2001

[28] "AGARD Flight Test Manual", Volume II: Stability and Control, Pergamon Press, 1959

[29] "Simplified Flutter Prevention Criteria for Personal Type Aircraft", Civil Aeronautics Administration, pre-1968

[30] "Fluid power with applications", A. Esposito, Prentice Hall, 1980, ISBN: 0-13-322701-4

[31] "Active flow control for reduction of unsteady stator-rotor interaction in a turbofan simulator", Jinwei Feng, Ph.D dissertation, Virginia Polytechnic Institute and State University, 2000

[32] "Basic research issues in aerodynamics, structural dynamics and control of high cycle fatigue". Air Force Office of Scientific Research. Workshop Held at Gas Turbine Laboratory, MIT, 1995.

[33] "Flutter and resonant vibration characteristics of the engine blades". A.V. Srinivasan. High Cycle Fatigue Workshop, MIT, 1995.

[34] "The aeroelastic response of a two dimensional airfoil with bilinear and cubic structural nonlinearities". H. Alighanbari, S.J. Price, B.H.K Lee, Journal of fluids and structures, Vol.9 No.2, 1995, pp.175-193

[35] "Metal Fatigue ", N.E. Frost, K.J. Marsh, L.P. Pook, Clarendon Press, 1974.

[36] "English Abstract Eng. vol 2", A. Wöhler, 1871.

[37] "The trouble with trim tabs", M.Richmond, Flight safety Australia, Sept.- October 1999

[38] "Mechanical engineering design", J.E. Shigly, L.D. Mitchell, 4th ed., McGraw Hill, NY, 1983

[39] "Limit Cycle Oscillation Characteristics of Fighter Aircraft", R.W. Bunton, and C.M Denegri, Jr. Journal of Aircraft, Vol. 37, No. 5, September-October 2000, pp. 916-918.

[40] "Limit Cycle Oscillation Flight Test Results of a Fighter with External Stores", C.M Denegri, Jr. Journal of Aircraft, Vol. 37, No. 5, September-October 2000, pp. 761-769.

[41] "Limit Cycle Oscillation and Flight Flutter Testing", W.J. Norton, Proceedings of the 21st Annual Symposium, Society of Flight Test Engineers, Lancaster, CA. 1990, pp. 3.4.4-3.4-12.

[42] "Residual Pitch Oscillation (RPO) Flight Test And Analysis on the B-2 Bomber", S.B. Jacobson, R.T. Britt, D.R. Dreim, and P.D. Kelly, AIAA Paper No. 98-1805, April 1998.

[43] "Simulation of Non-Linear Transonic Aeroelastic Behavior on the B-2", D.R. Dreim, S.B. Jacobson, and R.T. Britt, NASA CP-1999-209136 Part 2, CEAS/AIAA/ICASE/NASA Langley International Forum on Aeroelasticity and Structural Dynamics, USA, 1999, pp. 511-521.

[44] "Calculated Viscous and Scale Effects on Transonic Aeroelasticity", J.W. Edwards, Paper No. 1 in AGARD R-822, March 1998.

[45] "An analysis of the post-instability behavior of two-dimensional airfoil with a structural nonlinearity", S. Price, H. Alighanbari, B. Lee, Proceedings of the 34th AIAA/ASME/ASCE/AHS/ASC Structures, Structural dynamics and materials conference, pp.1452-1460.

[46] "The Structure and Properties of Materials, Vol. III", H.W. Hayden, W.G. Moffatt, and J. Wulff, John Wiley & Sons, 1965.

[47] "Fracture Mechanics from Theory to Practice", V.Z. Parton, Gordon and Breach Science Publishers

[48] "Physical Metallurgy Principles", Reed-Hill, Robert E, and R. Abbaschian. 3rd ed. Boston: PWS Publishing Company, 1994

[49] "Materials Science and Engineering, an Introduction", W.D Jr Callister,. 3rd ed. New York: John Wiley & Sons, Inc., 1994

[50] "High cycle fatigue damage accumulation in 6061-T6 Aluminum by probabilistic microplastic energy dissipation, R= -1", P. W. Whaley, T. J. George, P. Snell, Technical report: AFRL/PRTS, Propulsion and Power Short-Term R&D Support

[51] "A Fatigue Damage Approach for Life Prediction of MEMS Silicon Components", A.Varvani-Farahani, Submitted to Sensors and Actuators, 2003

[52] "Fatigue Response of Panels at Supersonic Flight Speeds", H. Alighanbari, A. Varvani-Farahani, Proceedings of 8th International Fatigue Congress, June 2002, Sweden, Vol. 1, pp. 149-157

[53] "Analyzing the fatigue crack growth in structural details", G.S. Wang, Engineering Fracture Mechanics, Vol. 53, No. 3, pp.345-361, 1996

[54] "Idealization of lug / pin contact pressures", B. Johnson of DAMT Ltd., www.nafems.org

[55] "Simple Rainflow Counting Algorithms", S. D.Downing, and D. F. Socie, International Journal of Fatigue, Vol. 4, N. 1, 1982, pp. 31-40

[56] "Standard Practices for Cycle Counting in Fatigue Analysis", ASTM E1049-85(1997), ASME 1985, American Society of Mechanical Engineers, USA.

[57] "Advanced fatigue fracture analysis", A. Varvani-Farahani, Ryerson University, Graduate course hand outs, Jan 2003

[58] "Aerospace alloy has been a huge success in golf club design", By J.M. Dahl and P.M. Novotny, Carpenter Technology Corp., Reading, PA, March 2002

17. Appendix

Some basic concepts and definitions are briefly given in this chapter.

17.1. Inertial Relief

Wing shear and bending is relieved by inertial loads due to the weight of the wing structure and various wing-mounted components. Each of these loads acts in the opposite sense to the aerodynamic lift, provided that the load factor (n) remains positive. This will include items such as weapons, systems, power plants, fuel tanks and the fuel itself.

17.2. Lift and Drag

The total aerodynamic force produced on a moving body is conventionally resolved into two components (Fig. 17.2.1): (i) Lift - perpendicular to airflow direction. (ii) Drag - parallel to airflow direction.

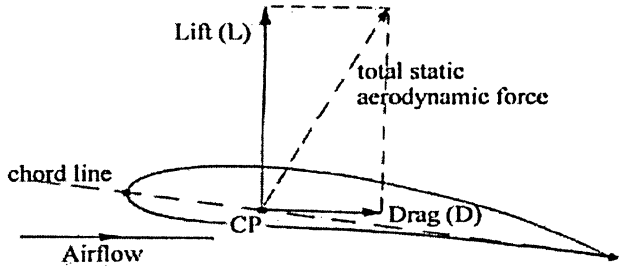

Fig. 17.2.1. Resolution of Total Aerodynamic Force into Lift and Drag Components

Lift and drag (and the total aerodynamic force) act through a point on the *chord line* of the body known as the *centre of pressure* (CP). Another important aeronautical engineering term that may be defined from Fig. 17.2.1 is the *angle of attack* (α), which is the angular difference between the airflow direction and chord line of the wing.

For an aircraft the lift force is the useful component and is effectively used to counter the aircraft's weight. The drag force is the penalty that has to be paid for producing lift and must be countered by an appropriately sustained thrust from a power plant system.

17.3. Origin of Lift

All that is needed to produce a lift force is an imbalance of the pressure distribution over the lower surface of the body relative to the upper surface (Fig. 17.3.1). In particular, the net

static pressure must be lower over the upper surface than over the lower surface; this will then resolve into an upwards lift force, perpendicular to the airstream direction, as per the definition of lift. To produce this pressure imbalance, a net airspeed difference is required and in particular, a faster moving airflow over the top surface than the bottom. Any flow situation whereby this occurs will result in a lift force being produced.

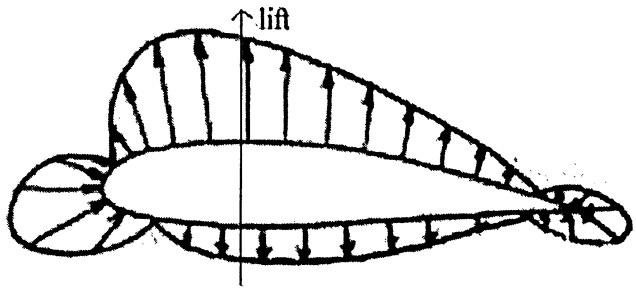

Fig. 17.3.1. Pressure Imbalance Causing Lift

In the case of a lifting airfoil or wing section, there are 2 means whereby the relative upper and lower surface airspeeds may be affected. Firstly, the section may be given *camber*, in which curvature is added (Fig. 17.3.2). *Positive* camber is where the section's mid-points lie above the *chord line* (the straight line joining the section's leading and trailing edges). Secondly, the section may be inclined to the oncoming airstream, i.e. given an *angle of attack.* In either case (or more usually a combination of the two), an airspeed difference will be produced and lift will occur.

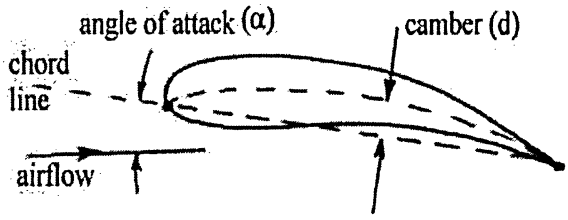

Fig. 17.3.2. Use of Camber and Angle of Attack to produce lift

It should be noted that the majority of the lift force is produced due to the low static pressure exerted on the upper surface rather than by high pressure on the lower surface. This means that the top surfaces of aircraft wings are especially critical to performance.

17.4. Wing Planform and Geometry - Definitions

Fig.17.4.1 makes it easier to elaborate some definitions:

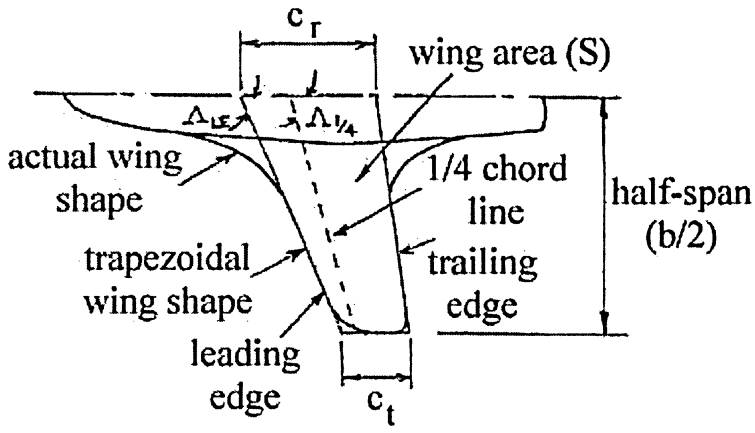

Fig. 17.4.1. Wing Geometry

Wing Area (S): usually based on an equivalent or reference *trapezoidal* planform which neglects the effects of leading edge and trailing edge extensions and also wing tip curvature. This section is extrapolated to the aircraft's centre-line to give a so-called *gross* planform area.

Wing Span (b): the tip-to-tip distance across the wing.

Wing Root Chord (c_r): the chord of the trapezoidal wing section taken at the aircraft centre-line.

Wing Tip Chord (c_t): the chord of the trapezoidal wing section taken at the wing tip.

Aspect Ratio (A or AR): the ratio of wing span to mean chord but may be defined more usefully as b^2 / S. The term is highly important as it is being frequently used throughout aerodynamics and aircraft design work.

17.5. Calculation Sheets

Calculations for Loading # 1

j=1, n_j=1, $\sigma_{min} = -150$ MPa, $\sigma_{max} = 450$ MPa,

$$\sigma_a = \frac{\sigma_{max} - \sigma_{min}}{2} = \frac{450+150}{2} = 300 \text{ MPa}, \qquad \sigma_m = \frac{\sigma_{max} + \sigma_{min}}{2} = \frac{450-150}{2} = 150 \text{ MPa}$$

$$S_e = \frac{\sigma_a}{1-\frac{\sigma_m}{\sigma_u}} = \frac{300}{1-\frac{150}{1233}} = 341.5 \text{ MPa},$$

$$N_{f.j.} = \frac{1}{2}\left(\frac{\sigma}{\sigma_f'}\right)^{\frac{1}{b}} = \frac{1}{2}\left(\frac{341.5}{2030}\right)^{\frac{1}{-0.104}} = 1.39x10^7 \text{ cycles to failure}$$

j=2, n_j=1, $\sigma_{min} = 150$ MPa, $\sigma_{max} = 300$ MPa,

$$\sigma_a = \frac{\sigma_{max} - \sigma_{min}}{2} = \frac{300-150}{2} = 75 \text{ MPa}, \qquad \sigma_m = \frac{\sigma_{max} + \sigma_{min}}{2} = \frac{300+150}{2} = 225 \text{ MPa}$$

$$S_e = \frac{\sigma_a}{1-\frac{\sigma_m}{\sigma_u}} = \frac{75}{1-\frac{225}{1233}} = 91.7 \text{ MPa},$$

$$N_{f.j.} = \frac{1}{2}\left(\frac{\sigma}{\sigma_f'}\right)^{\frac{1}{b}} = \frac{1}{2}\left(\frac{91.7}{2030}\right)^{\frac{1}{-0.104}} = 4.28x10^{12} \text{ cycles to failure}$$

j=3, n_j=1, $\sigma_{min} = -300$ MPa, $\sigma_{max} = 750$ MPa,

$$\sigma_a = \frac{\sigma_{max} - \sigma_{min}}{2} = \frac{750+300}{2} = 525 \text{ MPa}, \qquad \sigma_m = \frac{\sigma_{max} + \sigma_{min}}{2} = \frac{750-300}{2} = 225 \text{ MPa}$$

$$S_e = \frac{\sigma_a}{1-\frac{\sigma_m}{\sigma_u}} = \frac{525}{1-\frac{225}{1233}} = 642.2 \text{ MPa},$$

$$N_{f.j.} = \frac{1}{2}\left(\frac{\sigma}{\sigma_f'}\right)^{\frac{1}{b}} = \frac{1}{2}\left(\frac{642.2}{2030}\right)^{\frac{1}{-0.104}} = 31{,}994 \text{ cycles to failure}$$

$$N_f, total = \frac{1}{\frac{1}{1.39x10^7} + \frac{1}{4.28x10^{12}} + \frac{1}{31{,}994}} = 31{,}920 \text{ cycles to failure}$$

Calculations for Loading # 2

j=1, n_j=1, $\sigma_{\min} = -120$ MPa, $\sigma_{\max} = 360$ MPa,

$$\sigma_a = \frac{\sigma_{\max} - \sigma_{\min}}{2} = \frac{360+120}{2} = 240 \text{ MPa}, \qquad \sigma_m = \frac{\sigma_{\max} + \sigma_{\min}}{2} = \frac{360-120}{2} = 120 \text{ MPa}$$

$$S_e = \frac{\sigma_a}{1-\frac{\sigma_m}{\sigma_u}} = \frac{240}{1-\frac{120}{1233}} = 265.88 \text{ MPa},$$

$$N_{f.j.} = \frac{1}{2}\left(\frac{\sigma}{\sigma_f'}\right)^{\frac{1}{b}} = \frac{1}{2}\left(\frac{265.88}{2030}\right)^{\frac{1}{-0.104}} = 1.54x10^{8} \text{ cycles to failure}$$

j=2, n_j=1, $\sigma_{\min} = 120$ MPa, $\sigma_{\max} = 240$ MPa,

$$\sigma_a = \frac{\sigma_{\max} - \sigma_{\min}}{2} = \frac{240-120}{2} = 60 \text{ MPa}, \qquad \sigma_m = \frac{\sigma_{\max} + \sigma_{\min}}{2} = \frac{240+120}{2} = 180 \text{ MPa}$$

$$S_e = \frac{\sigma_a}{1-\frac{\sigma_m}{\sigma_u}} = \frac{60}{1-\frac{180}{1233}} = 70.26 \text{ MPa},$$

$$N_{f.j.} = \frac{1}{2}\left(\frac{\sigma}{\sigma_f'}\right)^{\frac{1}{b}} = \frac{1}{2}\left(\frac{70.26}{2030}\right)^{\frac{1}{-0.104}} = 5.56x10^{13} \text{ cycles to failure}$$

j=3, n_j=1, $\sigma_{\min} = -240$ MPa, $\sigma_{\max} = 600$ MPa,

$$\sigma_a = \frac{\sigma_{\max} - \sigma_{\min}}{2} = \frac{600+240}{2} = 420 \text{ MPa}, \qquad \sigma_m = \frac{\sigma_{\max} + \sigma_{\min}}{2} = \frac{600-240}{2} = 180 \text{ MPa}$$

$$S_e = \frac{\sigma_a}{1-\frac{\sigma_m}{\sigma_u}} = \frac{420}{1-\frac{180}{1233}} = 491.79 \text{ MPa},$$

$$N_{f.j.} = \frac{1}{2}\left(\frac{\sigma}{\sigma_f'}\right)^{\frac{1}{b}} = \frac{1}{2}\left(\frac{491.79}{2030}\right)^{\frac{1}{-0.104}} = 416{,}177 \text{ cycles to failure}$$

$$N_f, total = \frac{1}{\frac{1}{1.54x10^{8}} + \frac{1}{5.56x10^{13}} + \frac{1}{416{,}177}} = 415{,}055 \text{ cycles to failure}$$

Calculations for Loading # 3

j=1, n_j=1, $\sigma_{min} = -100$ MPa, $\sigma_{max} = 300$ MPa,

$$\sigma_a = \frac{\sigma_{max} - \sigma_{min}}{2} = \frac{300+100}{2} = 200 \text{ MPa}, \qquad \sigma_m = \frac{\sigma_{max} + \sigma_{min}}{2} = \frac{300-100}{2} = 100 \text{ MPa}$$

$$S_e = \frac{\sigma_a}{1 - \frac{\sigma_m}{\sigma_u}} = \frac{200}{1 - \frac{100}{1233}} = 217.65 \text{ MPa},$$

$$N_{f.j.} = \frac{1}{2}\left(\frac{\sigma}{\sigma_f'}\right)^{\frac{1}{b}} = \frac{1}{2}\left(\frac{217.65}{2030}\right)^{\frac{1}{-0.104}} = 1.06x10^{9} \text{ cycles to failure}$$

j=2, n_j=1, $\sigma_{min} = 100$ MPa, $\sigma_{max} = 200$ MPa,

$$\sigma_a = \frac{\sigma_{max} - \sigma_{min}}{2} = \frac{200-100}{2} = 50 \text{ MPa}, \qquad \sigma_m = \frac{\sigma_{max} + \sigma_{min}}{2} = \frac{200+100}{2} = 150 \text{ MPa}$$

$$S_e = \frac{\sigma_a}{1 - \frac{\sigma_m}{\sigma_u}} = \frac{50}{1 - \frac{150}{1233}} = 56.93 \text{ MPa},$$

$$N_{f.j.} = \frac{1}{2}\left(\frac{\sigma}{\sigma_f'}\right)^{\frac{1}{b}} = \frac{1}{2}\left(\frac{56.93}{2030}\right)^{\frac{1}{-0.104}} = 4.21x10^{14} \text{ cycles to failure}$$

j=3, n_j=1, $\sigma_{min} = -200$ MPa, $\sigma_{max} = 500$ MPa,

$$\sigma_a = \frac{\sigma_{max} - \sigma_{min}}{2} = \frac{500+200}{2} = 350 \text{ MPa}, \qquad \sigma_m = \frac{\sigma_{max} + \sigma_{min}}{2} = \frac{500-200}{2} = 150 \text{ MPa}$$

$$S_e = \frac{\sigma_a}{1 - \frac{\sigma_m}{\sigma_u}} = \frac{350}{1 - \frac{150}{1233}} = 398.48 \text{ MPa},$$

$$N_{f.j.} = \frac{1}{2}\left(\frac{\sigma}{\sigma_f'}\right)^{\frac{1}{b}} = \frac{1}{2}\left(\frac{398.48}{2030}\right)^{\frac{1}{-0.104}} = 3.15x10^{6} \text{ cycles to failure}$$

$$N_f, total = \frac{1}{\frac{1}{1.06x10^{9}} + \frac{1}{4.21x10^{14}} + \frac{1}{3.15x10^{6}}} = 3.14x10^{6} \text{ cycles to failure}$$

Calculations for Loading # 4

j=1, n_j=1, $\sigma_{min} = -50$ MPa, $\sigma_{max} = 150$ MPa,

$$\sigma_a = \frac{\sigma_{max} - \sigma_{min}}{2} = \frac{150+50}{2} = 100 \text{ MPa}, \qquad \sigma_m = \frac{\sigma_{max} + \sigma_{min}}{2} = \frac{150-50}{2} = 50 \text{ MPa}$$

$$S_e = \frac{\sigma_a}{1 - \frac{\sigma_m}{\sigma_u}} = \frac{100}{1 - \frac{50}{1233}} = 104.23 \text{ MPa},$$

$$N_{f.j.} = \frac{1}{2}\left(\frac{\sigma}{\sigma_f'}\right)^{\frac{1}{b}} = \frac{1}{2}\left(\frac{104.23}{2030}\right)^{\frac{1}{-0.104}} = 1.25x10^{12} \text{ cycles to failure}$$

j=2, n_j=1, $\sigma_{min} = 50$ MPa, $\sigma_{max} = 100$ MPa,

$$\sigma_a = \frac{\sigma_{max} - \sigma_{min}}{2} = \frac{100-50}{2} = 25 \text{ MPa}, \qquad \sigma_m = \frac{\sigma_{max} + \sigma_{min}}{2} = \frac{100+50}{2} = 75 \text{ MPa}$$

$$S_e = \frac{\sigma_a}{1 - \frac{\sigma_m}{\sigma_u}} = \frac{25}{1 - \frac{75}{1233}} = 26.62 \text{ MPa},$$

$$N_{f.j.} = \frac{1}{2}\left(\frac{\sigma}{\sigma_f'}\right)^{\frac{1}{b}} = \frac{1}{2}\left(\frac{26.62}{2030}\right)^{\frac{1}{-0.104}} = 6.28x10^{17} \text{ cycles to failure}$$

j=3, n_j=1, $\sigma_{min} = -100$ MPa, $\sigma_{max} = 250$ MPa,

$$\sigma_a = \frac{\sigma_{max} - \sigma_{min}}{2} = \frac{250+100}{2} = 175 \text{ MPa}, \qquad \sigma_m = \frac{\sigma_{max} + \sigma_{min}}{2} = \frac{250-100}{2} = 75 \text{ MPa}$$

$$S_e = \frac{\sigma_a}{1 - \frac{\sigma_m}{\sigma_u}} = \frac{175}{1 - \frac{75}{1233}} = 186.33 \text{ MPa},$$

$$N_{f.j.} = \frac{1}{2}\left(\frac{\sigma}{\sigma_f'}\right)^{\frac{1}{b}} = \frac{1}{2}\left(\frac{186.33}{2030}\right)^{\frac{1}{-0.104}} = 4.7x10^{9} \text{ cycles to failure}$$

$$N_f, total = \frac{1}{\frac{1}{1.25x10^{12}} + \frac{1}{6.28x10^{17}} + \frac{1}{4.7x10^{9}}} = 4.68x10^{9} \text{ cycles to failure}$$

Calculations for Loading # 5

j=1, n_j=1, $\sigma_{\min} = -10$ MPa, $\sigma_{\max} = 30$ MPa,

$$\sigma_a = \frac{\sigma_{\max} - \sigma_{\min}}{2} = \frac{30+10}{2} = 20 \text{ MPa}, \qquad \sigma_m = \frac{\sigma_{\max} + \sigma_{\min}}{2} = \frac{30-10}{2} = 10 \text{ MPa}$$

$$S_e = \frac{\sigma_a}{1 - \frac{\sigma_m}{\sigma_u}} = \frac{20}{1 - \frac{10}{1233}} = 20.16 \text{ MPa},$$

$$N_{f.j.} = \frac{1}{2}\left(\frac{\sigma}{\sigma_f'}\right)^{\frac{1}{b}} = \frac{1}{2}\left(\frac{20.16}{2030}\right)^{\frac{1}{-0.104}} = 9.09x10^{18} \text{ cycles to failure}$$

j=2, n_j=1, $\sigma_{\min} = 10$ MPa, $\sigma_{\max} = 20$ MPa,

$$\sigma_a = \frac{\sigma_{\max} - \sigma_{\min}}{2} = \frac{20-10}{2} = 5 \text{ MPa}, \qquad \sigma_m = \frac{\sigma_{\max} + \sigma_{\min}}{2} = \frac{20+10}{2} = 15 \text{ MPa}$$

$$S_e = \frac{\sigma_a}{1 - \frac{\sigma_m}{\sigma_u}} = \frac{5}{1 - \frac{15}{1233}} = 5.06 \text{ MPa},$$

$$N_{f.j.} = \frac{1}{2}\left(\frac{\sigma}{\sigma_f'}\right)^{\frac{1}{b}} = \frac{1}{2}\left(\frac{5.06}{2030}\right)^{\frac{1}{-0.104}} = 5.38x10^{24} \text{ cycles to failure}$$

j=3, n_j=1, $\sigma_{\min} = -20$ MPa, $\sigma_{\max} = 50$ MPa,

$$\sigma_a = \frac{\sigma_{\max} - \sigma_{\min}}{2} = \frac{50+20}{2} = 35 \text{ MPa}, \qquad \sigma_m = \frac{\sigma_{\max} + \sigma_{\min}}{2} = \frac{50-20}{2} = 15 \text{ MPa}$$

$$S_e = \frac{\sigma_a}{1 - \frac{\sigma_m}{\sigma_u}} = \frac{35}{1 - \frac{15}{1233}} = 35.43 \text{ MPa},$$

$$N_{f.j.} = \frac{1}{2}\left(\frac{\sigma}{\sigma_f'}\right)^{\frac{1}{b}} = \frac{1}{2}\left(\frac{35.43}{2030}\right)^{\frac{1}{-0.104}} = 4.02x10^{16} \text{ cycles to failure}$$

$$N_f, total = \frac{1}{\frac{1}{9.09x10^{18}} + \frac{1}{5.38x10^{24}} + \frac{1}{4.02x10^{16}}} = 4.00x10^{16} \text{ cycles to failure}$$

Calculations for Loading # 1.1

j=1, n_j=1, $\sigma_{min} = -150$ MPa, $\sigma_{max} = 750$ MPa,

$$\sigma_a = \frac{\sigma_{max} - \sigma_{min}}{2} = \frac{750+150}{2} = 450 \text{ MPa}, \qquad \sigma_m = \frac{\sigma_{max} + \sigma_{min}}{2} = \frac{750-150}{2} = 300 \text{ MPa}$$

$$S_e = \frac{\sigma_a}{1-\frac{\sigma_m}{\sigma_u}} = \frac{450}{1-\frac{300}{1233}} = 594.69 \text{ MPa},$$

$$N_{f.j.} = \frac{1}{2}\left(\frac{\sigma}{\sigma_f'}\right)^{\frac{1}{b}} = \frac{1}{2}\left(\frac{594.69}{2030}\right)^{\frac{1}{-0.104}} = 66{,}975 \text{ cycles to failure}$$

j=2, n_j=1, $\sigma_{min} = -100$ MPa, $\sigma_{max} = 800$ MPa,

$$\sigma_a = \frac{\sigma_{max} - \sigma_{min}}{2} = \frac{800+100}{2} = 450 \text{ MPa}, \qquad \sigma_m = \frac{\sigma_{max} + \sigma_{min}}{2} = \frac{800-100}{2} = 350 \text{ MPa}$$

$$S_e = \frac{\sigma_a}{1-\frac{\sigma_m}{\sigma_u}} = \frac{450}{1-\frac{350}{1233}} = 628.37 \text{ MPa},$$

$$N_{f.j.} = \frac{1}{2}\left(\frac{\sigma}{\sigma_f'}\right)^{\frac{1}{b}} = \frac{1}{2}\left(\frac{628.37}{2030}\right)^{\frac{1}{-0.104}} = 39{,}437 \text{ cycles to failure}$$

j=3, n_j=1, $\sigma_{min} = -100$ MPa, $\sigma_{max} = 800$ MPa,

$$\sigma_a = \frac{\sigma_{max} - \sigma_{min}}{2} = \frac{800+100}{2} = 450 \text{ MPa}, \qquad \sigma_m = \frac{\sigma_{max} + \sigma_{min}}{2} = \frac{800-100}{2} = 350 \text{ MPa}$$

$$S_e = \frac{\sigma_a}{1-\frac{\sigma_m}{\sigma_u}} = \frac{450}{1-\frac{350}{1233}} = 628.37 \text{ MPa},$$

$$N_{f.j.} = \frac{1}{2}\left(\frac{\sigma}{\sigma_f'}\right)^{\frac{1}{b}} = \frac{1}{2}\left(\frac{628.37}{2030}\right)^{\frac{1}{-0.104}} = 39{,}437 \text{ cycles to failure}$$

$$N_f, total = \frac{1}{\frac{1}{66{,}975} + \frac{1}{39{,}437} + \frac{1}{39{,}437}} = 15{,}233 \text{ cycles to failure}$$

Calculations for Loading # 2.1

j=1, n_j=1, σ_{min} = -120 MPa, σ_{max} = 600 MPa, $\sigma_a = \frac{\sigma_{max} - \sigma_{min}}{2} = \frac{600+120}{2} = 360$ MPa,

$$\sigma_m = \frac{\sigma_{max} + \sigma_{min}}{2} = \frac{600-120}{2} = 240 \text{ MPa}$$

$$S_e = \frac{\sigma_a}{1 - \frac{\sigma_m}{\sigma_u}} = \frac{360}{1 - \frac{240}{1233}} = 447.01 \text{ MPa},$$

$$N_{f.j.} = \frac{1}{2}\left(\frac{\sigma}{\sigma_f'}\right)^{\frac{1}{b}} = \frac{1}{2}\left(\frac{447.01}{2030}\right)^{\frac{1}{-0.104}} = 1.04x10^6 \text{ cycles to failure}$$

j=2, n_j=1, σ_{min} = -80 MPa, σ_{max} = 640 MPa, $\sigma_a = \frac{\sigma_{max} - \sigma_{min}}{2} = \frac{640+80}{2} = 360$ MPa,

$$\sigma_m = \frac{\sigma_{max} + \sigma_{min}}{2} = \frac{640-80}{2} = 280 \text{ MPa}, \quad S_e = \frac{\sigma_a}{1 - \frac{\sigma_m}{\sigma_u}} = \frac{360}{1 - \frac{280}{1233}} = 465.77 \text{ MPa},$$

$$N_{f.j.} = \frac{1}{2}\left(\frac{\sigma}{\sigma_f'}\right)^{\frac{1}{b}} = \frac{1}{2}\left(\frac{465.77}{2030}\right)^{\frac{1}{-0.104}} = 701{,}956 \text{ cycles to failure}$$

j=3, n_j=1, σ_{min} = -80 MPa, σ_{max} = 640 MPa, $\sigma_a = \frac{\sigma_{max} - \sigma_{min}}{2} = \frac{640+80}{2} = 360$ MPa,

$$\sigma_m = \frac{\sigma_{max} + \sigma_{min}}{2} = \frac{640-80}{2} = 280 \text{ MPa}, \quad S_e = \frac{\sigma_a}{1 - \frac{\sigma_m}{\sigma_u}} = \frac{360}{1 - \frac{280}{1233}} = 465.77 \text{ MPa},$$

$$N_{f.j.} = \frac{1}{2}\left(\frac{\sigma}{\sigma_f'}\right)^{\frac{1}{b}} = \frac{1}{2}\left(\frac{465.77}{2030}\right)^{\frac{1}{-0.104}} = 701{,}956 \text{ cycles to failure}$$

$$N_f, total = \frac{1}{\frac{1}{1.04x10^6} + \frac{1}{701{,}956} + \frac{1}{701{,}956}} = 262{,}566 \text{ cycles to failure}$$

Calculations for Loading # 3.1

j=1, n_j=1, σ_{min} = -100 MPa, σ_{max} = 500 MPa, $\sigma_a = \frac{\sigma_{max} - \sigma_{min}}{2} = \frac{500+100}{2} = 300$ MPa,

$$\sigma_m = \frac{\sigma_{max} + \sigma_{min}}{2} = \frac{500-100}{2} = 200 \text{ MPa}$$

$$S_e = \frac{\sigma_a}{1 - \frac{\sigma_m}{\sigma_u}} = \frac{300}{1 - \frac{200}{1233}} = 358.08 \text{ MPa},$$

$$N_{f.j.} = \frac{1}{2}\left(\frac{\sigma}{\sigma_f'}\right)^{\frac{1}{b}} = \frac{1}{2}\left(\frac{358.08}{2030}\right)^{\frac{1}{-0.104}} = 8.80x10^6 \text{ cycles to failure}$$

j=2, n_j=1, σ_{min} = -67 MPa, σ_{max} = 533 MPa, $\sigma_a = \frac{\sigma_{max} - \sigma_{min}}{2} = \frac{533+67}{2} = 300$ MPa,

$$\sigma_m = \frac{\sigma_{max} + \sigma_{min}}{2} = \frac{533-67}{2} = 233 \text{ MPa}, \quad S_e = \frac{\sigma_a}{1 - \frac{\sigma_m}{\sigma_u}} = \frac{300}{1 - \frac{233}{1233}} = 369.90 \text{ MPa},$$

$$N_{f.j.} = \frac{1}{2}\left(\frac{\sigma}{\sigma_f'}\right)^{\frac{1}{b}} = \frac{1}{2}\left(\frac{369.90}{2030}\right)^{\frac{1}{-0.104}} = 6.44x10^6 \text{ cycles to failure}$$

j=3, n_j=1, σ_{min} = -67 MPa, σ_{max} = 533 MPa, $\sigma_a = \frac{\sigma_{max} - \sigma_{min}}{2} = \frac{533+67}{2} = 300$ MPa,

$$\sigma_m = \frac{\sigma_{max} + \sigma_{min}}{2} = \frac{533-67}{2} = 233 \text{ MPa}, \quad S_e = \frac{\sigma_a}{1 - \frac{\sigma_m}{\sigma_u}} = \frac{300}{1 - \frac{233}{1233}} = 369.90 \text{ MPa},$$

$$N_{f.j.} = \frac{1}{2}\left(\frac{\sigma}{\sigma_f'}\right)^{\frac{1}{b}} = \frac{1}{2}\left(\frac{369.90}{2030}\right)^{\frac{1}{-0.104}} = 6.44x10^6 \text{ cycles to failure}$$

$$N_f, total = \frac{1}{\frac{1}{8.80x10^6} + \frac{1}{6.44x10^6} + \frac{1}{6.44x10^6}} = 2.36x10^6 \text{ cycles to failure}$$

Calculations for Loading # 4.1

j=1, n_j=1, σ_{min} = -50 MPa, σ_{max} = 250 MPa, $\sigma_a = \frac{\sigma_{max} - \sigma_{min}}{2} = \frac{250+50}{2} = 150$ MPa,

$$\sigma_m = \frac{\sigma_{max} + \sigma_{min}}{2} = \frac{250-50}{2} = 100 \text{ MPa}$$

$$S_e = \frac{\sigma_a}{1 - \frac{\sigma_m}{\sigma_u}} = \frac{150}{1 - \frac{100}{1233}} = 163.24 \text{ MPa},$$

$$N_{f.j.} = \frac{1}{2}\left(\frac{\sigma}{\sigma_f'}\right)^{\frac{1}{b}} = \frac{1}{2}\left(\frac{163.24}{2030}\right)^{\frac{1}{-0.104}} = 1.68x10^{10} \text{ cycles to failure}$$

j=2, n_j=1, σ_{min} = -33 MPa, σ_{max} = 267 MPa, $\sigma_a = \frac{\sigma_{max} - \sigma_{min}}{2} = \frac{267+33}{2} = 150$ MPa,

$$\sigma_m = \frac{\sigma_{max} + \sigma_{min}}{2} = \frac{267-33}{2} = 117 \text{ MPa}, \quad S_e = \frac{\sigma_a}{1 - \frac{\sigma_m}{\sigma_u}} = \frac{150}{1 - \frac{117}{1233}} = 165.73 \text{ MPa},$$

$$N_{f.j.} = \frac{1}{2}\left(\frac{\sigma}{\sigma_f'}\right)^{\frac{1}{b}} = \frac{1}{2}\left(\frac{165.73}{2030}\right)^{\frac{1}{-0.104}} = 1.45x10^{10} \text{ cycles to failure}$$

j=3, n_j=1, σ_{min} = -33 MPa, σ_{max} = 267 MPa, $\sigma_a = \frac{\sigma_{max} - \sigma_{min}}{2} = \frac{267+33}{2} = 150$ MPa,

$$\sigma_m = \frac{\sigma_{max} + \sigma_{min}}{2} = \frac{267-33}{2} = 117 \text{ MPa}, \quad S_e = \frac{\sigma_a}{1 - \frac{\sigma_m}{\sigma_u}} = \frac{150}{1 - \frac{117}{1233}} = 165.73 \text{ MPa},$$

$$N_{f.j.} = \frac{1}{2}\left(\frac{\sigma}{\sigma_f'}\right)^{\frac{1}{b}} = \frac{1}{2}\left(\frac{165.73}{2030}\right)^{\frac{1}{-0.104}} = 1.45x10^{10} \text{ cycles to failure}$$

$$N_f, total = \frac{1}{\frac{1}{1.68x10^{10}} + \frac{1}{1.45x10^{10}} + \frac{1}{1.45x10^{10}}} = 5.06x10^{9} \text{ cycles to failure}$$

Calculations for Loading # 5.1

j=1, n_j=1, σ_{min} = -10 MPa, σ_{max} = 50 MPa, $\sigma_a = \frac{\sigma_{max} - \sigma_{min}}{2} = \frac{50+10}{2} = 30$ MPa,

$$\sigma_m = \frac{\sigma_{max} + \sigma_{min}}{2} = \frac{50-10}{2} = 20 \text{ MPa}$$

$$S_e = \frac{\sigma_a}{1 - \frac{\sigma_m}{\sigma_u}} = \frac{30}{1 - \frac{20}{1233}} = 30.49 \text{ MPa},$$

$$N_{f.j.} = \frac{1}{2}\left(\frac{\sigma}{\sigma_f'}\right)^{\frac{1}{b}} = \frac{1}{2}\left(\frac{30.49}{2030}\right)^{\frac{1}{-0.104}} = 1.70x10^{17} \text{ cycles to failure}$$

j=2, n_j=1, σ_{min} = -6 MPa, σ_{max} = 54 MPa, $\sigma_a = \frac{\sigma_{max} - \sigma_{min}}{2} = \frac{54+6}{2} = 30$ MPa,

$$\sigma_m = \frac{\sigma_{max} + \sigma_{min}}{2} = \frac{54-6}{2} = 24 \text{ MPa}, \quad S_e = \frac{\sigma_a}{1 - \frac{\sigma_m}{\sigma_u}} = \frac{30}{1 - \frac{24}{1233}} = 30.60 \text{ MPa},$$

$$N_{f.j.} = \frac{1}{2}\left(\frac{\sigma}{\sigma_f'}\right)^{\frac{1}{b}} = \frac{1}{2}\left(\frac{30.60}{2030}\right)^{\frac{1}{-0.104}} = 1.65x10^{17} \text{ cycles to failure}$$

j=3, n_j=1, σ_{min} = -6 MPa, σ_{max} = 54 MPa, $\sigma_a = \frac{\sigma_{max} - \sigma_{min}}{2} = \frac{54+6}{2} = 30$ MPa,

$$\sigma_m = \frac{\sigma_{max} + \sigma_{min}}{2} = \frac{54-6}{2} = 24 \text{ MPa}, \quad S_e = \frac{\sigma_a}{1 - \frac{\sigma_m}{\sigma_u}} = \frac{30}{1 - \frac{24}{1233}} = 30.60 \text{ MPa},$$

$$N_{f.j.} = \frac{1}{2}\left(\frac{\sigma}{\sigma_f'}\right)^{\frac{1}{b}} = \frac{1}{2}\left(\frac{30.60}{2030}\right)^{\frac{1}{-0.104}} = 1.65x10^{17} \text{ cycles to failure}$$

$$N_f, total = \frac{1}{\frac{1}{1.70x10^{17}} + \frac{1}{1.65x10^{17}} + \frac{1}{1.65x10^{17}}} = 5.55x10^{16} \text{ cycles to failure}$$

Calculations for Loading # 6.1

j=1, n_j=1, σ_{min} = -350 MPa, σ_{max} = 300 MPa, $\sigma_a = \frac{\sigma_{max} - \sigma_{min}}{2} = \frac{300+350}{2} = 325$ MPa,

$$\sigma_m = \frac{\sigma_{max} + \sigma_{min}}{2} = \frac{300-350}{2} = -25 \text{ MPa}$$

$$S_e = \frac{\sigma_a}{1 - \frac{\sigma_m}{\sigma_u}} = \frac{325}{1 - \frac{-25}{1233}} = 318.54 \text{ MPa},$$

$$N_{f.j.} = \frac{1}{2}\left(\frac{\sigma}{\sigma_f'}\right)^{\frac{1}{b}} = \frac{1}{2}\left(\frac{318.54}{2030}\right)^{\frac{1}{-0.104}} = 2.71x10^7 \text{ cycles to failure}$$

j=2, n_j=1, σ_{min} = -550 MPa, σ_{max} = 100 MPa, $\sigma_a = \frac{\sigma_{max} - \sigma_{min}}{2} = \frac{100+550}{2} = 325$ MPa,

$$\sigma_m = \frac{\sigma_{max} + \sigma_{min}}{2} = \frac{100-550}{2} = -225 \text{ MPa}, \quad S_e = \frac{\sigma_a}{1 - \frac{\sigma_m}{\sigma_u}} = \frac{325}{1 - \frac{-225}{1233}} = 274.85 \text{ MPa},$$

$$N_{f.j.} = \frac{1}{2}\left(\frac{\sigma}{\sigma_f'}\right)^{\frac{1}{b}} = \frac{1}{2}\left(\frac{274.85}{2030}\right)^{\frac{1}{-0.104}} = 1.12x10^8 \text{ cycles to failure}$$

j=3, n_j=1, σ_{min} = -550 MPa, σ_{max} = 100 MPa, $\sigma_a = \frac{\sigma_{max} - \sigma_{min}}{2} = \frac{100+550}{2} = 325$ MPa,

$$\sigma_m = \frac{\sigma_{max} + \sigma_{min}}{2} = \frac{100-550}{2} = -225 \text{ MPa}, \quad S_e = \frac{\sigma_a}{1 - \frac{\sigma_m}{\sigma_u}} = \frac{325}{1 - \frac{-225}{1233}} = 274.85 \text{ MPa},$$

$$N_{f.j.} = \frac{1}{2}\left(\frac{\sigma}{\sigma_f'}\right)^{\frac{1}{b}} = \frac{1}{2}\left(\frac{274.85}{2030}\right)^{\frac{1}{-0.104}} = 1.12x10^8 \text{ cycles to failure}$$

$$N_f, total = \frac{1}{\frac{1}{2.71x10^7} + \frac{1}{1.12x10^8} + \frac{1}{1.12x10^8}} = 1.83x10^7 \text{ cycles to failure}$$